Reviews in Mineralogy & Geochemistry
Vol. 61, pp. 557-607, 2006

Reactivity of Sulfide Mineral Surfaces

Kevin M. Rosso

Chemical Sciences Division
and W.R. Wiley Environmental Molecular Sciences Laboratory
Pacific Northwest National Laboratory
Richland, Washington, U.S.A.
e-mail: kevin.rosso@pnl.gov

David J. Vaughan

School of Earth Atmospheric and Environmental Sciences
and Williamson Research Centre for Molecular Environmental Science
University of Manchester
Manchester, United Kingdom
e-mail: david.vaughan@manchester.ac.uk

INTRODUCTION

In the preceding chapter, the fundamental nature of sulfide mineral surfaces has been discussed, and the understanding we have of the ways in which the surface differs from a simple truncation of the bulk crystal structure reviewed. This naturally leads on to considering our understanding of sulfide surface chemistry, in the sense of how sulfide surfaces interact and react, particularly with gases and liquids.

As noted elsewhere in this volume, research on sulfide mineral surfaces and surface reactivity is a relatively recent concern of mineralogists and geochemists, partly prompted by the availability of new imaging and spectroscopic methods, powerful computers and new computer algorithms. There has been a significantly longer history of sulfide mineral surface research associated with technologists working with, or within, the mining industry. Here, electrochemical methods, sometimes combined with analytical and spectroscopic techniques, have been used to probe surface chemistry. The motivation for this work has been to gain a better understanding of the controls of leaching reactions used to dissolve out metals from ores, or to understand the chemistry of the froth flotation systems used in concentrating the valuable (usually sulfide) minerals prior to metal extraction.

The need for improved metal extraction technologies is still a major motivation for research on sulfide surfaces, but in the last couple of decades, new concerns have become important drivers for such work. In particular, much greater awareness of the negative environmental impact of acid and toxic metal-bearing waters derived from breakdown of sulfide minerals at former mining operations has prompted research on oxidation reactions, and on sorption of metals at sulfide surfaces. At the interface between fundamental geochemistry and industrial chemistry, the role of sulfide substrates in catalysis, and in the self-assembly and functionalization of organic molecules, has become an area of significant interest. Such work ranges in its application from the development of new industrial processes, to fundamental questions of the possible role of sulfide surfaces in catalyzing the formation of the complex organic molecules leading to the emergence of life on Earth.

In this chapter, we aim to provide an overview of current understanding of sulfide surface chemistry. The size of this research field is already such that it is impossible to discuss all

1529-6466/06/0061-0010$10.00 DOI: 10.2138/rmg.2006.61.10

of the published work, but key examples are considered and readers directed to the main literature sources. The chapter begins with some examples of reaction with gaseous species (O_2, H_2O, H_2S, CH_3OH) as these are the most accessible in terms of understanding reactivity at the molecular scale. The very important oxidation and related electron transfer reactions, in both air and aqueous solution, are then considered before considering examples of catalysis and functionalization/self-assembly and interaction with organic molecules. In the final section, sorption of metal ions onto sulfide mineral surfaces is discussed before a few words concerning the future outlook for research in this entire area.

ELEMENTARY ADSORPTION/OXIDATION REACTIONS

The reaction of clean mineral surfaces with pure gaseous molecules in a highly controlled UHV environment can provide important insights into the reactivity of particular surfaces and surface sites. In this way, reaction mechanisms can be explored experimentally for different cleavage or fracture surfaces and types of defect sites, and with close control of temperature and concentration of the reactant molecule. Computer modeling approaches, including *ab initio* computations, are well suited to the theoretical investigation of such reactions. Examples of experimental and computational studies of key sulfide surfaces will now be discussed, before considering the complexities of more advanced surface transformation reactions with air and with aqueous solutions of varying compositions.

Galena

As emphasized in the preceding chapter, the simple crystal structure and perfect cleavage of PbS have made it an attractive substance for surface science studies, and this extends to work on surface reactivity. In particular, the surface breakdown reactions in oxidizing conditions on exposure to water have been a focus of attention because of their obvious environmental relevance. A more fundamental understanding of these reactions is possible through both experimental and computer modeling studies of the interaction of oxygen atoms or molecular species such as H_2O with the dominant cleavage (and growth) surface of galena, the (100) surface.

While a significant body of experimental work has been performed on PbS oxidation in air and aqueous solutions, as reviewed in the next section, very little work has been performed under the controlled conditions of UHV. Therefore, much of what is currently known about the initial adsorption and oxidation reactions due to oxygen exposure comes from a combination of scanning tunneling microscopy (STM) and spectroscopy (STS) studies of the initial stages of oxidation in air and computational molecular modeling. Eggleston and Hochella were the first to show atomic-scale evidence of PbS (100) oxidation due to air exposure (Eggleston and Hochella 1990, 1991, 1993, 1994). Using STM, they showed that nanometer-scale oxidation patches (low tunneling current dark areas) develop on this surface that interrupt the otherwise continuous array of high tunneling current sites (bright spots) corresponding to atomic positions. Becker and Hochella (1996) used *ab initio* computation methods to calculate STM images, STS spectra and X-ray photoelectron spectra (XPS) peak shifts for pristine PbS (100) and for that surface following reaction with oxygen. Experimental STM images of the upper valence band of galena show a periodic array of spots which could arise from either Pb or S; the calculations show that these spots (imaged under conditions where electrons tunnel from occupied states) stem from electronic states with sulfur 3*p* character near the Fermi level. If the galena is exposed to oxygen, more and more of the former bright sulfur spots appear as dark spots. Zyubina et al. (2005) recently demonstrated mechanisms of O_2 dissociation on small PbS (and doped and undoped PbTe) clusters via a peroxide-like surface complex using density functional theory (DFT) cluster calculations. A combination of periodic slab and aperiodic cluster calculations showed that dissociated O_2 yields O adsorbed on top of terrace S atoms, and O migrating beneath the uppermost surface planes at steps and corners (Becker and Hochella 1996; Zyubina et al. 2005).

Computation of STS spectra as well as STM images help in understanding how these reactions would manifest in experimental tunneling data. In STS measurements, the microscope tip is held stationary over a certain atomic position and the bias voltage ramped over a range (e.g., −1 V to +1 V). Under certain conditions and simplifications, the tunneling spectra provide information reflecting the local density of states of the sample at the location of the tip (Tersoff and Hamann 1985). Figure 1 shows a calculated STM image and calculated STS spectra for a sulfur atom with an oxygen adsorbed on top, its second nearest neighbor atom, and a third sulfur atom least affected by the adsorbed oxygen. The depletion of electron density associated with oxygen atom adsorption can be seen in the calculated spectra and accounts for the darkening of regions in the STM image where adsorption has occurred. This effect results from electron density being drawn away from the surface sulfurs by the oxygen atom, depopulating the S 3*p* states (oxidizing the sulfide). This interpretation of STM images was subsequently confirmed experimentally by Eggleston (1997) on PbS (100) surfaces oxidized in air using a dual-bias imaging method which enables simultaneous acquisition of two kinds of images (one of occupied and one of unoccupied states) over a single area of the surface. This showed that S 3*p* states are depopulated by oxidation and so (under negative sample bias) fewer electrons tunnel from these states into the STM tip, giving a darkened area; conversely, when the bias is reversed electrons tunnel from the tip to the sample and oxidized sites appear bright.

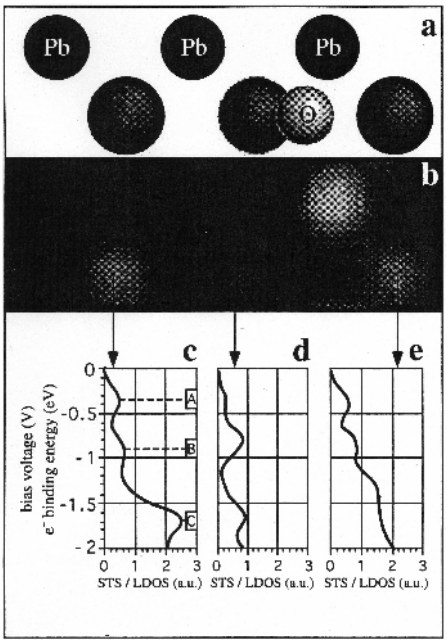

Figure 1. Calculated PbS (100) STM image and STS spectra with adsorbed oxygen; a) the supercell unit for the calculation, b) the calculated image, c-e) calculated spectra at various locations. [Used by permission of Elsevier from Becker and Hochella (1996), *Geochimica et Cosmochimica Acta*, Vol. 60, Fig. 7, p. 2421.]

The PbS (100) surface is particularly amenable to both experimental and computational studies and has therefore become a system for demonstrating new concepts in mineral surface science. The combined experimental and computational work of Becker and Rosso (2001) on geometric and electronic structures of step edges on this surface have been discussed in the previous chapter (Rosso and Vaughan 2006) and clearly have important implications for surface reactivity. Those results show that the density and energy of empty Pb 6*p* states is significantly increased at step edge Pb sites relative to that of terrace Pb sites. This suggests that the edge Pb sites have increased capacity to accept electrons, and are therefore stronger Lewis acid sites. Therefore charge donating adsorbates such as water should bind more strongly to these sites via σ-like interaction between water O sp^3 and surface Pb 6*p* orbitals. This is similar to the earlier findings of Wright et al. (1999a,b) who employed *ab initio* cluster and periodic models to investigate specifically the reaction of water on the PbS surface. They found that the perfect (100) surface is very unreactive, even in the presence of vacancies in the surface layer. However, at step sites (of a single atomic layer), a dissociation reaction described by:

$$PbS + H_2O \rightarrow Pb(OH)^+ + HS^- \quad (1)$$

was calculated to occur readily, even at ambient temperature. These calculations also provided insights into the reaction mechanism. In Figure 2, the initial configuration, the transition state geometry, and the dissociated end-product structure from the calculations are shown. In a further development of this work, Bryce et al. (2000) used an embedded cluster model adjoined to a dielectric conductor screening model and included the effects of bulk water via a reaction field. The results are in line with the earlier studies and suggest that physisorption occurs at the perfect (100) surface and chemisorption at a step defect. The effect of the polarization and dynamics of surrounding solvent water tends to reduce the driving force and increase the reaction barrier for water dissociation at steps (barrier = 48.6 kcal mol^{-1}).

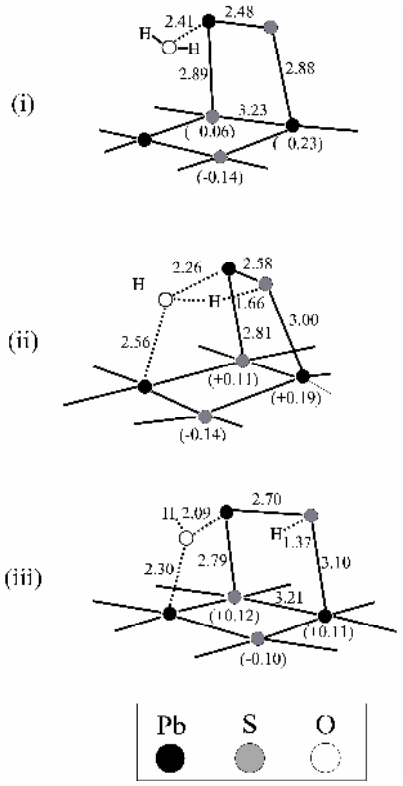

Figure 2. Computational model for H_2O interaction at a PbS (100) step site showing the (i) initial, (ii) transition-state, and (iii) final configurations. [Used by permission of Elsevier from Wright et al. (1999a), *Chemical Physics Letters*, Vol. 299, Fig. 1, p. 529.]

Another aspect of surface reactivity developed using galena as a model (and also pyrite) is the so-called "proximity effect" on semiconducting mineral surfaces using *ab initio* molecular orbital and planewave DFT calculations, and STM and STS experiments (Becker et al. 2001; Rosso and Becker 2003). Here, the concept is one whereby the chemical reaction of one surface site influences the electronic structure and reactivity of neighboring or nearby sites. The site-to-site interaction of interest here is indirect through the surface, rather than the more well-known direct through-space interadsorbate interaction (such as described by the Fowler adsorption isotherm). The example involving galena which was studied initially was its oxidation via interaction with ferric iron and water. In this case, Fe^{3+} acts as the oxidizing agent (electron acceptor) and water promotes the reaction and supplies the oxygen necessary to produce sulfate in the overall reaction (after Rimstidt et al. 1994):

$$PbS + 8Fe^{3+} + 4H_2O \leftrightarrow Pb^{2+} + SO_4^{2-} + 8H^+ + 8Fe^{2+} \quad (2)$$

It is shown by Becker et al. (2001) that the ferric iron and the water molecule involved in this oxidation do not have to be bonded to the same surface atom. As illustrated in Figure 3, these species may interact at different surface sites including step sites, and electrons may be transported through mineral surface layers or along specific pathways such as steps over distances of several nanometers. Rosso and Becker (2003) used planewave DFT calculations to assess the strength of through-surface interadsorbate interaction between oxygen adsorbed on PbS (100) and also between adsorbed oxygen and vacancies as a function of separation distance. Energy-distance plots indicate that the proximity effect becomes a very strong attractive interaction at separations decreasing below ~5-6 Å, and the proximity effect persists at separations up to 12 Å for these surface species (Fig. 4). Interestingly, the strength of the proximity effect attracting adsorbed O atoms together was found to out-compete their through-space electrostatic repulsion. This finding demonstrated the presence of a strong organizing

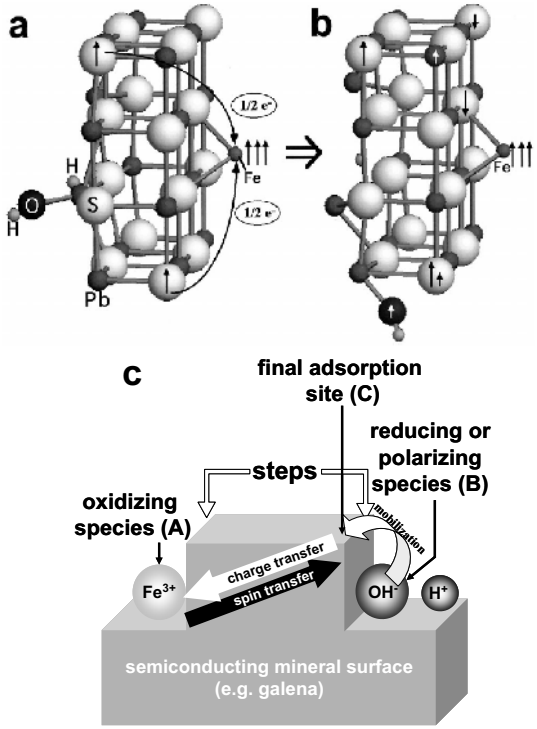

Figure 3. Galena as an example of the proximity effect on semiconducting mineral surfaces, showing a) a cluster model with the initial configuration, b) final configuration, and c) a diagram depicting the relevant processes. [Used by permission of Elsevier from Becker et al. (2001), *Geochimica et Cosmochimica Acta*, Vol. 65, Figs. 1 and 2, pp. 2643 and 2644.]

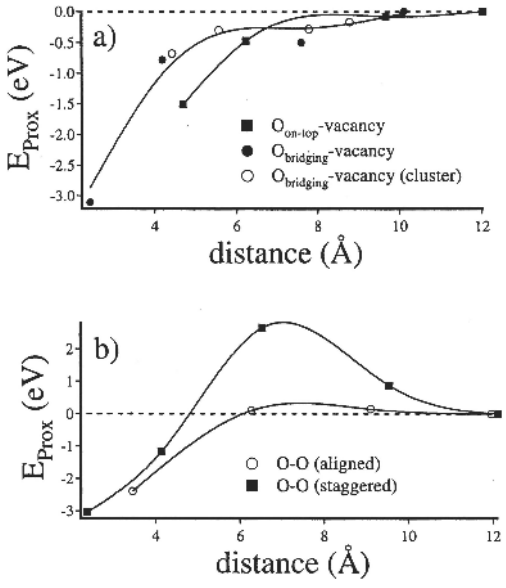

Figure 4. Calculated proximity effect energies as a function of distance of separation for a) adsorbed oxygen-vacancy interaction, and b) oxygen-oxygen interaction on PbS (100). [Used with permission of Elsevier from Rosso et al. (2003), *Geochimica et Cosmochimica Acta*, Vol. 67, Fig. 9, p. 949.]

force on like adatoms that could explain the oxidation of galena and possibly other sulfide surfaces by progressive patchwork growth.

Pyrite

Experimental studies of pyrite surface reactivity are more demanding than those for galena, given that it is more difficult to isolate crystallographically-oriented pyrite surfaces. Pyrite has poor (100) cleavage, and thus fracture leads to macroscopically conchoidal surfaces. However, as reviewed in the previous chapter (Rosso and Vaughan 2006), true pyrite (100) surfaces can be found on fracture surfaces at length scales of several hundred nanometers. Therefore, while crystallographic pyrite surfaces are accessible by local probe methods such as STM, most analytical surface spectroscopic methods necessarily incorporate the overall complicated surface structure. The surface topography and preparation method are particularly key issues for understanding the reactivity of pyrite surfaces because of the wide range of site types and structural environments that occur on differently prepared surfaces.

Using an *in situ* UHV cleaning approach developed by Strongin and co-workers (Chaturvedi et al. 1996), seminal investigations have been undertaken on clean natural pyrite *growth* surfaces for the study of reaction with gaseous molecules in UHV. The cleaning procedure involves cycling between low-energy sputtering, usually with He^+, to remove adventitious material and annealing. These "as-grown" surfaces were shown to be very topographically complex as observed by atomic force microscopy (Hochella et al. 1998), but this cleaning approach gives sharp (100) diffraction as determined by low-energy electron diffraction (LEED). In-UHV fracturing also leads to sharp (100) diffraction, but the topography is distinctly different (Rosso et al. 1999a). The in-UHV cleaned surfaces present a smaller population of monosulfide species than surfaces prepared by in-UHV fracture (Chaturvedi et al. 1996). The cleaning approach has the advantage that it is amenable to preparing pyrite surfaces of orientation other than (100) for UHV study, such as the (111) surface, whereas surfaces of this orientation have not yet been shown to be produced to any degree by fracture. Nevertheless, some differences between the reactivity of pyrite surfaces prepared by in-UHV cleaning and in-UHV fracture are readily apparent in the literature. In general, both sets of results re-enforce the importance of defects, their structure and relative abundance, for controlling at least the initial stages of pyrite surface reactivity.

Guevremont et al. (1997, 1998a,b,c,d) employed a range of UHV surface analytical techniques including XPS and temperature programmed desorption (TPD) to study the interaction of molecular H_2O, O_2 and CH_3OH on cleaned pyrite growth surfaces. The binding of H_2O and CH_3OH at low temperature (90 K) was investigated by techniques including TPD and photoemission of adsorbed xenon (PAX) (Guevremont et al. 1997) which show that both species adsorb molecularly at 90 K and thermally desorb between 170 and 400 K. The PAX data led to the suggestion that adsorption of these molecules occurs preferentially at small populations of defect sites believed to be, at least in part, sulfur vacancies. After defect sites are saturated, it is suggested that adsorbates cluster on the less reactive stoichiometric surface.

Guevremont (1998a) made comparative studies of the oxidation of in-UHV cleaned (100) and (111) growth surfaces exposed to H_2O, O_2 and an H_2O/O_2 mixture in an apparatus allowing surfaces to be reacted at environmentally relevant pressures and then studied using XPS. In these experiments, neither the (100) nor the (111) growth surface exhibited substantial reaction in pure O_2 for exposure pressures up to 1 bar. Exposure to H_2O vapor at similar pressures resulted in significant oxidation of FeS_2 (111) but a much smaller amount of oxidation of the FeS_2 (100) surface; it was suspected by the authors that on the (100) surface, H_2O only reacted at defect sites. Both surfaces showed substantial reaction with the H_2O/O_2 mixture, and this was more than the sum of reactions observed with equivalent amounts of pure H_2O and O_2, leading to the suggestion of a "synergy" between H_2O and O_2 in oxidizing pyrite. Typical XPS data (S 2*p* and Fe 2*p* peaks) for the fresh FeS_2 (100) surface and that exposed to H_2O, O_2 or

mixed H_2O/O_2 are shown in Figure 5. In the S 2*p* spectra, features at binding energies of 162.5 and 161.5 eV from the clean surface are assigned to the disulfide group and a monosulfide species; after exposure to H_2O or H_2O/O_2, new features appear at higher binding energies of 163.4 and 168.8 eV whereas equivalent exposure to O_2 has no significant effect. Although these features are clearly products of the oxidation reactions, their precise assignment is uncertain although polysulfide, a sulfur oxide or thiosulfate are suggested as possible reaction products. The growth of a feature at 711 eV in the Fe 2*p* spectrum, following oxidation, was attributed to Fe^{3+}, possibly associated with an iron oxide or hydroxide surface product.

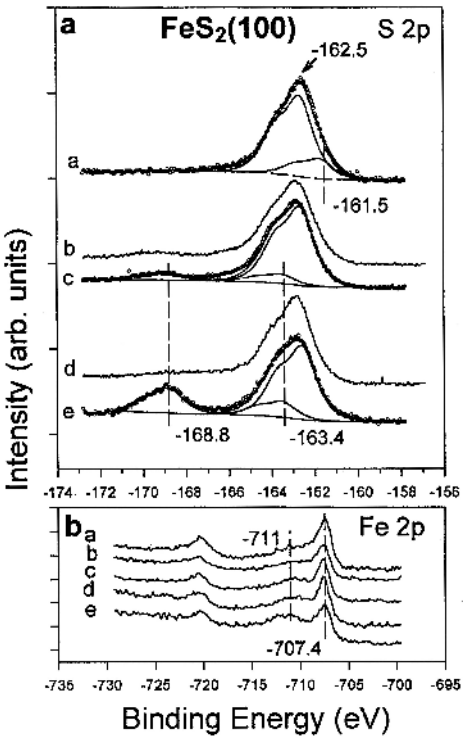

Figure 5. XPS data for pyrite exposed to various amounts of pure or mixtures of O_2 and H_2O, showing changes in the a) S 2*p* and b) Fe 2*p* spectra. From Guevremont et al. (1998b).

Reactivity studies using precision reactant exposures in UHV with pyrite surfaces generated by fracturing in vacuum demonstrate behavior that is somewhat different than that for cleaned growth surfaces. For example, in contrast to the results of Guevremont et al. (1998a) on cleaned growth surfaces, several studies have shown that fractured pyrite surfaces react with pure O_2. High resolution STM imaging, STS spectra, and ultraviolet photoelectron spectroscopy (UPS) along with quantum mechanical cluster calculations were used by Rosso et al. (1999b) to study fundamental oxidation mechanisms when gaseous O_2 and H_2O and their mixtures interact with pyrite (100) surfaces. The UPS data for surfaces exposed to O_2 show that the density of states decreases at the top of the valence band but increases deeper in the valence band, indicating consumption of low binding energy electrons occupying dangling bond surface states localized on surface Fe atoms, consistent with the formation of Fe^{3+}-O^- bonds. This was observable by UPS for O_2 exposures as low as 4 L (e.g., 10^{-7} mbar exposure for 40 seconds); the oxidation process stopped at 20 L (Fig. 6). For exposures to pure H_2O, no oxidation was observed for exposures up to 10 L. Similar to the results of Guevremont et al. (1998a) however, it was found that a mixture of O_2 and H_2O oxidizes the surface much more than does an equivalent concentration of pure O_2 (Fig. 6).

Kendelewicz et al. (2004) have studied FeS_2 fracture surfaces exposed to pure O_2, water vapor, and air using SR-XPS and found behavior largely consistent with Rosso et al. (1999b). Molecular oxygen reacts to a measurable extent with the surface through dissociative chemisorption of O_2 (Fig. 7) but they found this to occur only at much higher O_2 exposures (~10^7 L). These authors went to exposures up to atmospheric O_2 partial pressures. They also found the surface to be unreactive with pure water vapor up to exposures similar to room temperature saturation pressures (~10^{10} L). Consistent with Guevremont et al. (1998a), Kendelewicz et al. (2004) showed the presence of a small percentage of surface monosulfide, which is eradicated by dosing with either O_2 or H_2O. They also identified a range of intermediate oxidation products in their experiments including sulfur oxoanions and zero-valent sulfur.

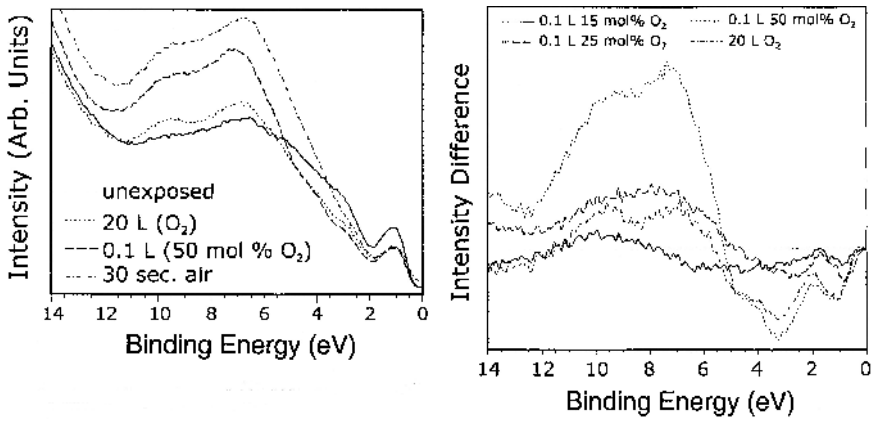

Figure 6. He I UPS valence band spectra (left) and difference spectra (right) comparing pristine pyrite surfaces with those exposed to O_2, O_2-H_2O, and air. From Rosso et al. (1999b).

The progressive oxidation of the (100) surface was experimentally followed at the local atomic level (Rosso et al. 1999b). UHV STM images at atomic resolution were obtained for (100) terraces of the surface exposed to O_2 and to H_2O/O_2 mixtures (Fig. 8). The images show oxidation features in the form of dark "patches" in both the upper valence band and lower conduction band states around the Fermi level. On the basis of *ab initio* calculations discussed below, these features are interpreted as where dissociative chemisorption of O_2 has taken place at Fe sites. At these sites, Fe $3d_{z^2}$ dangling bond surface state density has been lost to bonds with the chemisorbed O species. Consistent with the UPS data, STS spectra show removal of the highest occupied and lowest unoccupied surface state density associated with dangling bond states, in accordance with this interpretation.

The importance of Fe $3d_{z^2}$-like surface states in controlling the initial stages of pyrite (100) reaction with O_2 and H_2O has been re-enforced by various computational molecular modeling studies. The interaction between pyrite (100) surfaces and water molecules is a well-studied example. Hartree-Fock, DFT, and empirical potential models all show that H_2O molecules at various coverages preferentially adsorb by association between their oxygen atoms and surface Fe atoms (Rosso et al. 1999b; de Leeuw et al. 2000; Stirling et al. 2003; Philpott et al. 2004). This result is consistent with experiments (Pettenkofer et al. 1991; Guevremont et al. 1997, 1998a; Rosso et al. 1999b; Kendelewicz et al. 2004). Empirical potential calculations on slab models by de Leeuw et al. (2000) predicted an adsorption energy of –47 kJ mol^{-1}, which compares well with –42 kJ mol^{-1} determined by TPD (Guevremont et al. 1998a). In particular, this interaction has been shown to be mediated by charge transfer from highest occupied O $2p$ states in water to unoccupied Fe $3d_{z^2}$ electronic states near the Fermi level (Rosso et al. 1999b; Stirling et al. 2003). H_2O dissociation is predicted to be strongly unfavorable (Rosso et al. 1999b; de Leeuw et al. 2000; Stirling et al. 2003; Philpott et al. 2004) and partly stabilized at higher coverages by hydrogen bonding interactions (Stirling et al. 2003). Occupied Fe $3d_{z^2}$ states are responsible for binding adsorbed O_2 and providing electrons that destabilize the O_2 molecule towards dissociation by electron transfer from surface Fe into π^* antibonding O_2 molecular orbitals (Rosso et al. 1999b). These authors also showed that H_2O dissociatively sorbs at surface Fe sites only when dissociated O_2 is present at Fe sites nearby, which provides a mechanism explaining the enhanced reactivity of the combined O_2/H_2O gases in causing surface oxidation (Fig. 9). Collectively from the spectroscopic data, STM data, and molecular modeling results to date, the supported synergistic oxidation mechanism is one involving competitive adsorption of O_2 and

H_2O at surface Fe sites, oxidation of surface Fe sites by O_2, dissociation of co-adsorbed H_2O at Fe sites, and charge redistribution in surface S atoms (Rosso et al. 1999b). This is one pathway that allows for production of hydroxyls from dissociated water and subsequent nucleophilic attack of these hydroxyls at surface S sites, consistent with the observations that oxygen in final product sulfate arises predominantly from water molecules (Taylor et al. 1984; Usher et al. 2004, 2005).

AIR/AQUEOUS OXIDATION

The instability of sulfide minerals when exposed to the Earth's atmosphere or to oxygenated surface waters makes redox reactions in general, and oxidation reactions in particular, of great importance in sulfide mineralogy and geochemistry. As seen from the work on clean surfaces and pure gases (O_2, H_2O) or simple mixtures (H_2O/O_2) discussed above, progress has been made in studies of "model systems" from which the importance of oxygen and water as oxidants is clear. In natural systems, and in the engineered environments associated with the mineral processing industry, other oxidants are important (notably ferric iron) and other factors commonly make major contributions to the rates of redox reactions. In particular, temperature and pH conditions are significant, and the roles played by a range of bacteria are especially important. In the following section, oxidation in the air and redox reactions under a variety of conditions are discussed with reference to three major binary sulfide minerals (galena, pyrite and pyrrhotite), one mixed cation sulfide (chalcopyrite) and one mixed anion sulfide (arsenopyrite).

Galena

Earlier work on the oxidation of galena in air and in aqueous solution was summarized in Tossell and Vaughan (1987); subsequent work has involved electrochemical methods (e.g., Richardson and Odell 1984; Fornasiero et al. 1994), Raman spectroscopy (Turcotte et al. 1993), thermodynamic methods (Acharya and Paul 1991; Janczuk et al. 1992a,b) and the use of bacteria (Bang et al. 1995). XPS has proved particularly important in providing insights into oxidation processes, more recently through XPS using synchrotron radiation (SR-XPS).

Laajalehto et al. (1997) have applied SR-XPS to air oxidized galena and found that this provides an order of magnitude improvement in surface sensitivity compared with conventional XPS through the ability to tune the energy of the source. After only 10 min

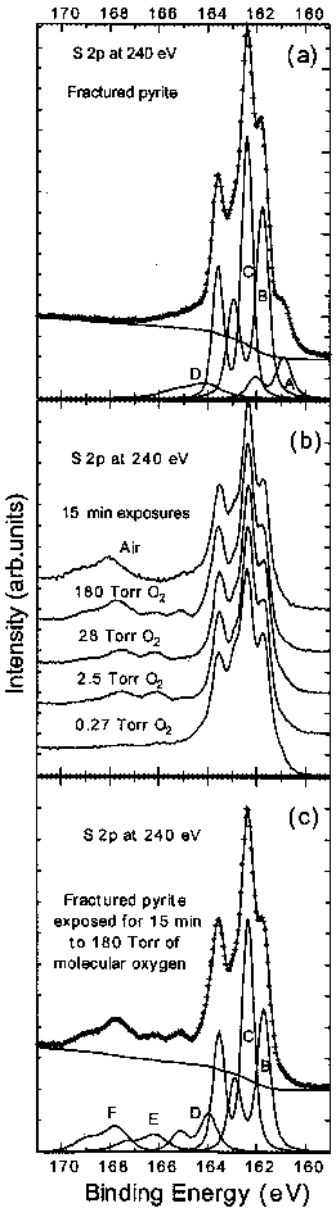

Figure 7. S 2*p* SR-XPS data for a) fractured pyrite, b) after exposure to different partial pressures of O_2 and to ambient air, and c) after exposure to 180 Torr of O_2 for 15 min. [Used with permission of Elsevier from Kendelewicz et al. (2004) *Surface Science*, Vol. 558, Fig. 1, p. 82.]

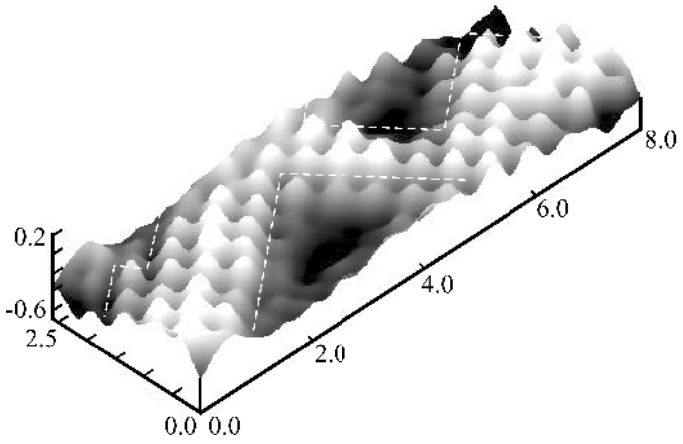

Figure 8. UHV STM image of a pyrite (100) surface exposed to 4 L O_2, showing oxidized patches as low dark areas outlined by white dashed lines. Unoxidized Fe sites affected by neighboring oxidized sites and the still unaffected regions. Scale bars are in nanometers. Adapted from Rosso et al. (1999b).

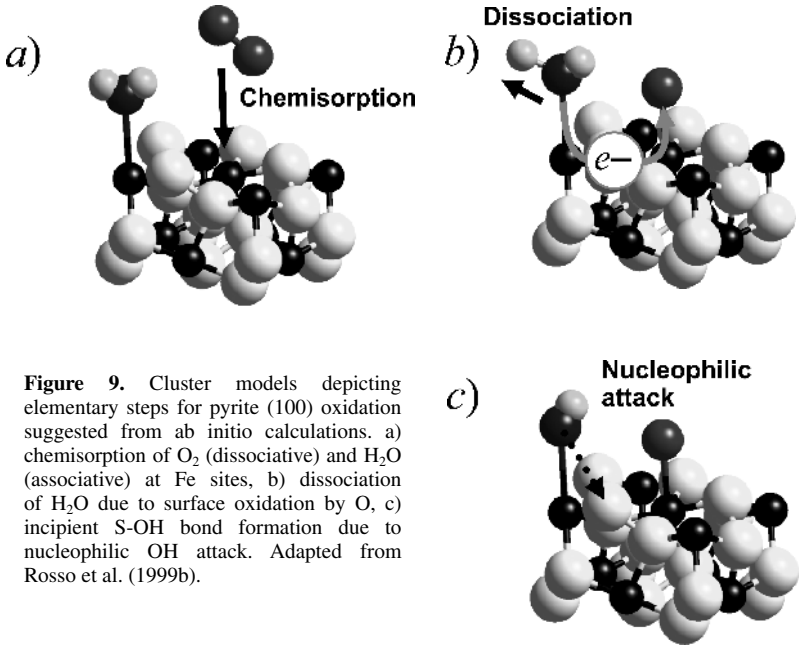

Figure 9. Cluster models depicting elementary steps for pyrite (100) oxidation suggested from ab initio calculations. a) chemisorption of O_2 (dissociative) and H_2O (associative) at Fe sites, b) dissociation of H_2O due to surface oxidation by O, c) incipient S-OH bond formation due to nucleophilic OH attack. Adapted from Rosso et al. (1999b).

exposure to air, oxidized sulfur (both sulfate and metal polysulfide) species can be found, and oxidized sulfur and lead species are observed simultaneously, supporting congruent oxidation of the surface. The kinetics of PbS oxidation contrasts with that of pyrite which was also studied. Whereas a layer of oxidation products forms on pyrite after only a few seconds, it takes several minutes for any evidence of galena oxidation to appear. However, whereas the instantly formed layer on pyrite seems to passivate the surface, on galena, oxidation proceeds continuously with time. Laajalehto et al. (1997) have also drawn attention to the

importance of cooling samples of sulfides such as galena before and during XPS experiments (both conventional and SR-XPS) to avoid loss of volatile surface reaction products. Their examination (*ex situ* and over the temperature range 143 – 298 K) of S 2*p* spectra of an electrochemically oxidized PbS (100) surface showed a layer structure of elemental sulfur and metal polysulfides.

Other more recent studies of galena oxidation have also used vibrational spectroscopies to identify oxidation products. Shapter et al. (2000) used Raman spectroscopy to identify oxysulfates ($PbO{\cdot}PbSO_4$, $3PbO{\cdot}PbSO_4$ and $4PbO{\cdot}PbSO_4$) produced by laser heating in air. (Unfortunately the temperatures involved, suggested to reach 900ºC, could not be exactly determined). Chernyshova (2003) used *in situ* FTIR to study the products of electrochemical oxidation of galena formed at the electrode/electrolyte interface in solution at pH 9.2. From the FTIR measurements it is suggested that under these conditions oxidation of galena starts with the reaction:

$$PbS + 2xh^+ \rightarrow Pb_{1-x}S + xPb^{2+} \quad (3)$$

followed by the reaction:

$$PbS + 2h^+ \rightarrow Pb^{2+} + S^0 \quad (4)$$

where h^+ denotes a hole. Lead sulfate, thiosulfate and polythionate ions are formed from the elementary sulfur formed at the first oxidation stage, and $Pb(OH)_2$ is precipitated (Fig. 10).

Pyrite

The importance of the oxidation of pyrite in air and aqueous media has ensured numerous studies, both experimental and theoretical. Earlier work has been reviewed by Lowson (1982), and amongst many subsequent studies have been those of McKibben and Barnes (1986), Buckley and Woods (1987), Moses et al. (1987), Mishra and Osseo-Asare (1992), Moses and Herman (1991), Raikar and Thurgate (1991), Karthe et al. (1993), Tao et al. (1994), Sasaki (1994), Nesbitt and Muir (1994), Williamson and Rimstidt (1994), Ciminelli and Osseo-Asare (1995), Eggleston et al. (1996), Bonnissel-Gissinger et al. (1998), Evangelou et al. (1998), Schaufuss et al. (1998a,b), England et al. (1999), Kelsall et al. (1999), Chernyshova (2003), Todd et al. (2003), Rimstidt and Vaughan (2003), Abraitis et al. (2004), and Mattila et al. (2004).

More recent work on pyrite oxidation in air has benefited from the application of synchrotron-based spectroscopic methods (see above discussion of Kendelewicz et al. 2004, and also Laajalehto et al. 1997; Schaufuss et al. 1998a,b; Mattila et al. 2004). For example, Schaufuss et al. (1998a,b) using SR-XPS were able to demonstrate the presence of at least three distinct sulfur states at the fractured pyrite surface, each of which oxidizes at a different rate in air. The most reactive surface component is S^{2-} and the second, the surface atom of the first disulfide layer (S_2^{2-}) with sulfur atoms of disulfide groups beneath the surface layer (bulk coordinated sulfurs) being least reactive. A model for the oxidation mechanism based on that originally proposed by Eggleston et al. (1996) was put forward by Schaufuss et al. (1998b) and is illustrated in Figure 11. In this model, Fe^{3+} states are proposed to arise after fracturing of S-S bonds (as suggested by Nesbitt et al. 1998) by electron transfer from Fe^{2+} to this S^- state which then reacts rapidly to sulfate. In turn the sulfate may be displaced from its original site (bonded to Fe^{3+}) as a result of competitive sorption of H_2O, O_2 and OH^-. In Figure 11, the adsorption of O_2 as an outer sphere complex is shown. The initial stages in the formation of an Fe_2O_3 overlayer may begin with the transfer of an electron from an adjacent Fe^{2+} to the Fe^{3+} center, followed by electron transfer to O_2 producing O_2^- and the formation of Fe^{3+}-O bonds. This produces a second Fe^{3+}. Based on bulk band edge positions of pyrite and hematite, Eggleston et al. (1996) argued that Fe^{2+} in surface Fe_2O_3 patches is a better O_2 reductant than Fe^{2+} in pyrite (Fig. 12). They proposed electron migration through Fe_2O_3 "surface states" to

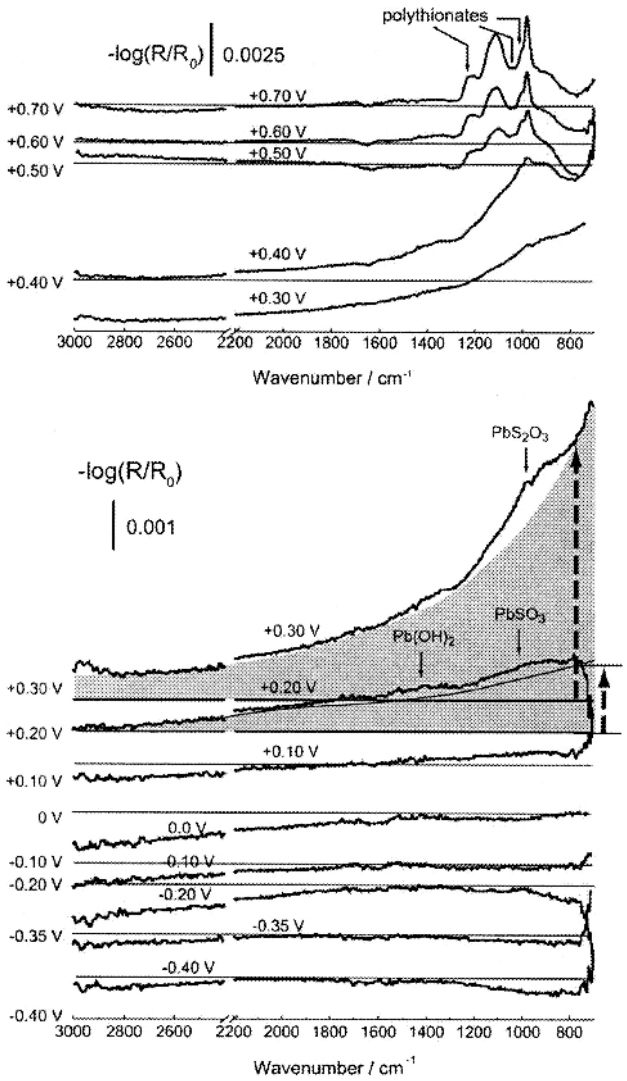

Figure 10. FTIR-ATR difference spectra of the PbS (100) / solution interface measured in situ during an electrochemical positive potential scan at pH 9.2 showing the formation of lead sulfate, thiosulfate, polythionate, and other reaction products. [Used with permission of Elsevier from Chernyshova (2003), *Journal of Electroanalytical Chemistry*, Vol. 558, Fig. 2, p. 87.]

O_2 and facile Fe^{2+}/Fe^{3+} cycling at patch edges by this mechanism. Ultimately, the result is the build-up of islands of Fe^{3+} oxides across the pyrite surface (Eggleston et al. 1996).

The products of pyrite oxidation in aqueous environments are critically dependent upon solution chemistry, with evidence of reaction products formed under different conditions coming from a wide range of (mostly *ex situ*) analytical techniques. For example, England et al. (1999) used synchrotron-based glancing-angle X-ray absorption spectroscopy to probe the surface (~2-3 nm) region of pyrite oxidized at pH 9.2, finding a goethite-like surface species. Todd et al. (2003) used synchrotron-based X-ray absorption spectroscopy (using oxygen *K*- and sulfur and

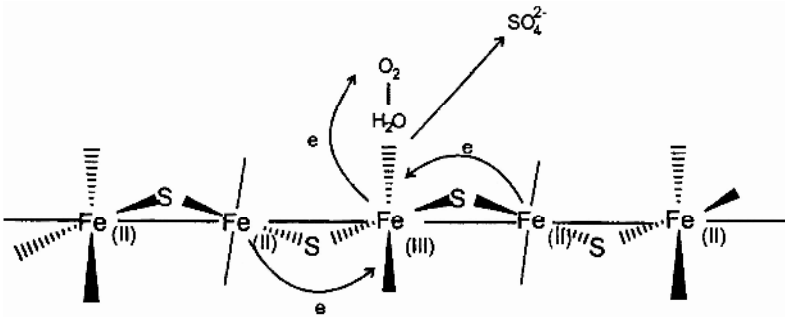

Figure 11. Proposed reaction mechanism of pyrite oxidation in air. [Used with permission of Elsevier from Schaufuss et al. (1998b), *Surface Science*, Vol. 411, Fig. 3, p. 327.]

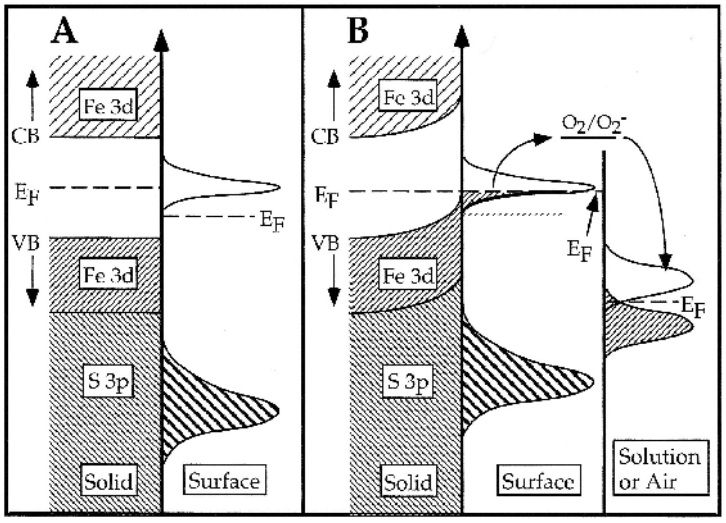

Figure 12. Band structure of the bulk and surface of pyrite a) before and b) after equilibration including the effects of hematite-like conduction band (unfilled) and valence band (bold cross-hatched) surface states. Surface oxidation in air leads to hematite-like surface states that facilitate further electron transfer to O_2. From Eggleston et al. (1996).

iron *L*-edges) to determine the phases formed by oxidation in aqueous electrolytes at pH 2 to pH 10 in the top 2-5 nm region of the surface. Below pH 4 a ferric (hydroxyl) sulfate is the main product whereas at higher pH an Fe^{3+} oxyhydroxide is also found. The presence of Fe^{3+} in solution autocatalyzes the oxidation, promoting ferric oxyhydroxide formation at low pH. Under the most alkaline conditions, the O *K*-edge spectrum resembles that of goethite (cf. England et al. 1999). Very similar results were found by Bonnissel-Gissinger et al. (1998) concerning the pH dependence of reaction products. Chernyshova (2003), in an *in situ* FTIR study in aqueous solution, looked at the earlier stages of reaction with the first (monolayer) stage (above 0 V in pH 9.2 solution) producing elemental sulfur and ferric hydroxide and the second (at 0.4 V) producing a sub-monolayer of Fe^{3+}-OH surface species. At higher potentials bulk ferric hydroxide, ferric sulfite and polythionates were reported, accompanied thereafter by sulfate formation. In another FTIR study, Evangelou et al. (1998) explored the role of bicarbonate in solution and suggested the formation of carbonate complexes at the pyrite surface.

Of course, the redox chemistry of pyrite in aqueous solution presents far more complexities than that involving pure gases or air. As noted by Rimstidt and Vaughan (2003), the key controls of mechanisms and hence rates of the oxidation of pyrite remain poorly understood, despite many decades of research, because the processes of aqueous oxidation involve a complex series of elementary reactions. As pointed out by Basolo and Pearson (1967), the elementary steps of redox reactions almost always involve the transfer of only one electron at a time, so that oxidation of a disulfide such as pyrite to release sulfate requires transfer of seven electrons and, hence, up to seven elementary steps. Furthermore, the minerals are semiconductors, so that the reactions are electrochemical in nature and, as already considered above in discussing the proximity effect, various reactions can happen at different sites with electron transfer through the mineral. Following arguments put forward by Kelsall et al. (1999) and Rimstidt and Vaughan (2003), it is suggested that pyrite aqueous oxidation is an electrochemical process with three distinct steps, as illustrated in Figure 13. These are the: (1) cathodic reaction, (2) electron transport, and (3) anodic reaction. The cathodic reaction involves an aqueous species that accepts electrons from an Fe^{2+} site on the mineral surface, such as O_2 in the reaction:

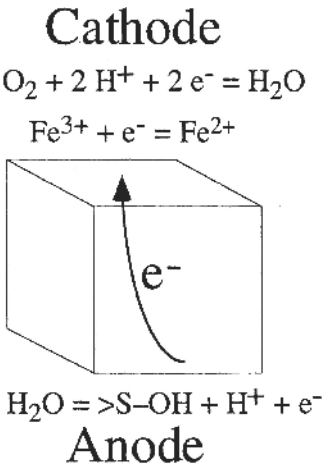

Figure 13. Diagram showing three steps involved in pyrite oxidation in aqueous solution. The cathodic reaction transfers electrons from the surface to the oxidant, which are replenished by electrons collected from anodic surface sites. Water molecules react with sulfur atoms around the anodic surface sites to form sulfoxy species, releasing hydrogen ions into solution. [Used with permission of Elsevier from Rimstidt and Vaughan (2003), *Geochimica et Cosmochimica Acta*, Vol. 67, Fig. 1, p. 874.]

$$FeS_2 + {}^7/_2O_2 + H_2O \rightarrow Fe^{2+} + 2H^+ + 2SO_4^{2-} \quad (5)$$

It is now clear that the cathodic reaction is the rate-determining step for sulfide mineral oxidation. Williamson and Rimstidt (1994) showed that the pyrite oxidation rate depends on concentration of O_2 or another oxidant (such as Fe^{3+}) and this is the case for other sulfide minerals such as galena, sphalerite, chalcopyrite and arsenopyrite. The exact stages involved in a reaction such as that above are suggested to follow a sequence like that already outlined above for air oxidation. The anodic reaction involves a multistep sulfur atom oxidation (electron removal) process with a sequence of surface reactions of the type:

$$py\text{-S-S} = py\text{-S-S}^+ + e^- \quad (6)$$

$$py\text{-S-S}^+ + H_2O = py\text{-S-S-OH} + H^+ \quad (7)$$

$$py\text{-S-S-OH} = py\text{-S-SO} + e^- + H^+ \quad (8)$$

$$py\text{-S-SO} = py\text{-S-SO}_2 + 2e^- + 2H^+ \quad (9)$$

$$py\text{-S-SO}_2 = py\text{-S-SO}_3 + 2e^- + 2H^+ \quad (10)$$

At this stage there is a tendency for this species to break away from the surface as a thiosulfate complex, which can be written as

$$py\text{-S-S-O}_3 = py + MS_2O_3 \quad (11)$$

The final step is envisaged as being pH dependent so, if the pH is high, the terminal $S\text{-}SO_3$ completely ionizes making the S-S bond stronger than the Fe-S bond, so much of the sulfur is released into solution as $S_2O_3^{2-}$. At low pH, the majority of terminal $S\text{-}SO_3$ groups retain a

proton (so are S-SO_3H) which encourages transfer of electrons into the S-S bond where they are more easily transferred to the cationic site, leaving the sulfur with a very positive charge. This leads to further nucleophilic attack by a water molecule to produce SO_4^{2-}.

Pyrrhotite

A broad review of pyrrhotite oxidation has been published by Belzile et al. (2004), including data on oxidation rates, activation energies and factors controlling rates and oxidation products, as well as discussion of oxidation mechanisms. The air oxidation of pyrrhotite was studied using XPS by Buckley and Woods (1985) and they proposed a mechanism involving diffusion of iron to the surface to form (via an Fe^{2+} oxide) an Fe^{3+} hydrated oxide/hydroxide outer layer. Very detailed XPS and Auger electron spectroscopy (AES) studies of pyrrhotite (Fe_7S_8) air oxidation by Pratt et al. (1994) and Mycroft et al. (1995b) confirm this outward diffusion of iron. These authors propose the development of a layer structure with (after 50 h of air oxidation) an oxygen-rich and sulfur-depleted outermost layer of <1 nm covering an iron-deficient, sulfur-rich layer which, in turn, shows a gradual decrease in S:Fe ratio with depth. The proposed inward sequence of compositions is $FeO_{1.5}$, FeS_2, Fe_2S_3 and Fe_7S_8. A mechanism is proposed whereby molecular oxygen is adsorbed onto the pyrrhotite surface and reduced to O^{2-} and then reacts with Fe^{3+} bonded to S to form Fe^{3+}-O bonds and Fe^{3+} oxyhydroxides. Diffusion of iron outwards establishes the outer ferric oxyhydroxide layer, causing the depletion and chemical stratification of the underlying sulfide. Mycroft et al. (1995b) used angle resolved XPS to refine this model, suggesting approximate thicknesses of ~5 Å for the oxidized layer and 30 Å for the S-depleted sulfide layer. In both this work and secondary ion mass spectrometry (SIMS) studies by Smart et al. (2000), S-S bonding was observed and interpreted as due to reorganization of the pyrrhotite structure towards a marcasite-type structure in the proposed FeS_2 layer.

Chalcopyrite

Chalcopyrite ($CuFeS_2$) as the most important copper ore mineral, has been the subject of numerous studies of its surface reactivity, particularly of its oxidation in air and redox reactions in aqueous solution. Yin et al. (1995) quantitatively estimated the extent of atmospheric oxidation by determining the charge required to electrochemically reduce chalcopyrite exposed to air for different time periods. The average thickness of the oxidized surface layer was found to develop from ~1.5 nm after 10 min to ~4.5 nm after 100 min. Studies in solution have commonly used electrochemical techniques, and a brief résumé of the results obtained from many of these investigations is provided by Yin et al. (2000).

Typical of the results of such studies is the cyclic voltammogram in Figure 14 which shows a series of peaks arising from oxidation reactions leading to the breakdown of the chalcopyrite in an alkaline solution at pH 9.2, typical of flotation systems (Yin et al. 2000). Although inferences can be drawn directly from the electrochemical data as to the reactions giving rise to peaks A, B and C in the voltammogram, independent information on the phases forming at the chalcopyrite electrode surface can only be obtained from surface analysis. Thus, following transfer of an electrode conditioned under the appropriate potential into the analysis chamber of an XPS instrument, carefully avoiding exposure to atmosphere, O 1*s* and Fe 2*p* photoelectron spectra (Fig. 15) can be used to confirm that ferric oxide/hydroxide and some adsorbed O_2 are present under the conditions associated with the first oxidation reaction (A in Fig. 14). The S 2*p* and Cu 2*p* spectra remain essentially unchanged from those of the fresh surface. Combining electrochemical and spectroscopic data for reaction A, and then for the oxidation reactions at higher potentials (peaks B and C in Fig. 14) enables a sequence of oxidation reactions to be proposed:

$$2CuFeS_2 + 6xOH^- \rightarrow 2CuFe_{1-x}S_2 + xFe_2O_3 + 3xH_2 + 6xe^- \quad (12)$$

$$2CuFeS_2 + 6OH^- \rightarrow 2CuS_2^* + Fe_2O_3 + 3H_2O + 6e^- \quad (13)$$

$$CuFeS_2 + 3OH^- \rightarrow CuS_2^* + Fe(OH)_3 + 3e^- \quad (14)$$

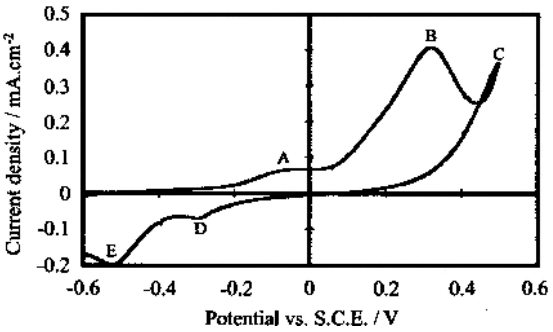

Figure 14. Cyclic voltammogram for oxidation reactions on chalcopyrite in a 0.1 M $Na_2B_4O_7$, pH 9.2 solution at 298 K. The potential was swept at 20 mV/s. See text for discussion of peaks. [Used with permission of The Mineralogical Society from Vaughan et al. (2002), *Mineralogical Magazine*, Vol. 66, Fig. 4a, p. 660.]

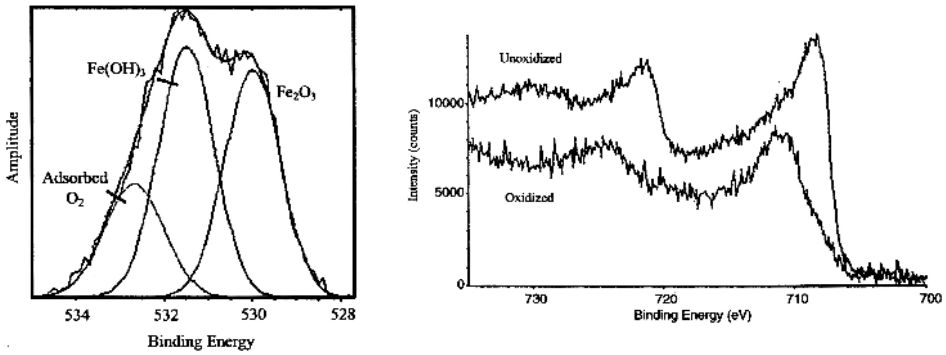

Figure 15. XPS spectra of the O 1*s* (left) and Fe 2*p* (right) regions on an electrochemically oxidized chalcopyrite surface. [Used with permission of The Mineralogical Society from Vaughan et al. (2002), *Mineralogical Magazine*, 66, Vol. Fig. 4b,c, pp. 660-661.]

The implications of these reactions are that at potentials just above the rest potential, a monolayer of $Fe_2O_3/Fe(OH)_3$ is formed leaving Cu and S unoxidized in the original chalcopyrite structure as a metastable phase of CuS_2 stoichiometry (and designated CuS_2*). Together these phases cause passivation of the surface. A simple model of the development of the surface during oxidation is shown in Figure 16. With increasing potential these reactions continue, removing Fe from deeper within the chalcopyrite and with solid state diffusion being the likely rate-controlling mechanism. Above a critical potential, the metastable CuS_2* phase decomposes (Yin et al. 2000). The oxidation of chalcopyrite in solution at pH 4 appears to be a similar story to that under alkaline conditions, with an iron oxide/hydroxide "layer" forming at the surface (Farquhar et al. 2003). However, AFM studies of the oxidized surface, both *ex situ* and in the presence of the fluid, show the presence of islands (<0.15 μm wide) of reaction products (Fig. 17). Coverage of the surface with these islands increases with the amount of charge passed. In a study of chalcopyrite oxidation in alkaline solutions, the findings of which were in general agreement with the above, Velasquez et al. (2005) observed similar "islands" using SEM (with EDX analysis facility). They describe the surface as composed of a "very superficial heterogeneous layer of oxidized materials from which protrude islands formed by grains of oxide, hydroxide and sulfate materials."

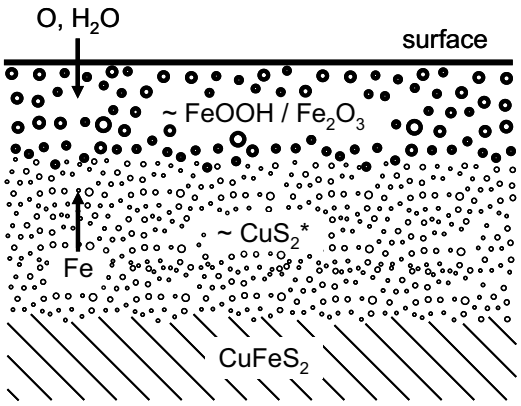

Figure 16. Model for the development of the chalcopyrite surface during oxidation. [Redrawn from Vaughan et al. 2002.]

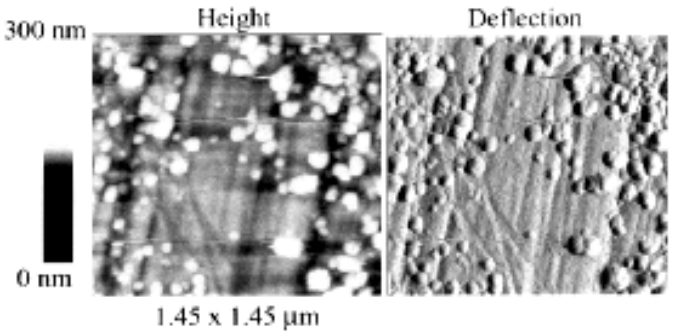

Figure 17. AFM height (left) and deflection (right) images of a chalcopyrite surface electrochemically oxidized at 650 mV in pH 4 solution. [Used with permission of The Mineralogical Society from Vaughan et al. (2002), *Mineralogical Magazine*, Vol. 66, Fig. 4f, p. 661.]

Similar electrochemical and XPS studies of the metal-enriched ("stuffed") derivatives of chalcopyrite, talnakhite ($Cu_9Fe_8S_{16}$), mooihoekite ($Cu_9Fe_9S_{16}$) and haycockite ($Cu_4Fe_5S_8$), show marked differences in oxidation rates compared with the stoichiometric phase (Vaughan et al. 1995). This is to be expected if solid state diffusion is the rate controlling mechanism; the additional interstitial site metals in the stuffed derivatives would be more active and mobile. The relative rates of oxidation are in the order haycockite > mooihoekite > talnakhite > chalcopyrite for reaction in acid solution. In alkaline solutions a similar pattern is observed although, following initial rapid oxidation of the stuffed derivatives, the passivating film which forms retards further oxidation to a greater extent than in chalcopyrite.

Arsenopyrite

A substantial number of studies have been performed to investigate the reactivity of arsenopyrite (FeAsS) in air and in aqueous solutions representative of both environmental systems and mineral processing operations (e.g., Buckley and Walker 1988; Richardson and Vaughan 1989; Nesbitt et al. 1995; Fernandez et al. 1996a,b; Nesbitt and Muir 1998; Schaufuss et al. 2000; Costa et al. 2002; Jones et al. 2003; Mikhlin and Tomashevich 2005). Many of these involve electrochemical methods and XPS studies, although Mikhilin and Tomashevich (2005) used X-ray absorption near-edge spectroscopy (XANES) as a surface probe. Jones et al. (2003) are among the first to investigate microbially mediated surface oxidation reactions, and Schaufuss et al. (2000) further exploit the potential of SR-XPS.

The earlier studies largely employed conventional XPS and AES analysis of fresh surfaces of natural arsenopyrite and of the same surfaces exposed to air, water and a range of acid and alkali aqueous solutions, as well as electrochemical treatments. For example, Buckley and Walker (1988) found that initial oxidation of FeAsS in air occurs rapidly according to the following generalized reaction:

$$FeAsS + (¾x + ½by)O_2 \rightarrow ½xFe_2O_3 + yAsO_b + Fe_{1-x}As_{1-y}S \ (y > x;\ b \leq 1.5) \qquad (15)$$

with arsenic being oxidized faster than iron, and subsequent oxidation being slower and leading to the formation of As^{5+} oxides.

The complexities of the pristine FeAsS surface, showing a range of different As and S surface sites as revealed by SR-XPS, have already been discussed elsewhere in this volume (Rosso and Vaughan 2006). The same synchrotron technique was also used by Schaufuss et al. (2000) to study the initial stages of arsenopyrite oxidation on exposure to pure oxygen. The spectra show fast oxidation of As surface sites, and a consecutive reaction scheme for arsenic oxidation involving one-electron transfer steps was indicated by the detection of As^0, As^{2+}, As^{3+} and As^{5+} (Fig. 18). Further oxidation included exposure to the laboratory atmosphere (< 30 min) with the acquired spectra showing As^{5+} to be the final arsenic oxidation product, and with sulfate being the final result of S oxidation (but with numerous intermediate products). These oxidation products reach the surface by diffusion from the bulk. The authors also produced data interpreted in terms of the development of oxidized surface overlayers; an arsenic and iron containing overlayer on exposure to pure O_2 and, following atmospheric oxidation, another layer on top of this with an approximate FeOOH composition. This Fe-O overlayer was estimated to be ~1.8 monolayers thick and formed by the interaction of (atmospheric) water with Fe surface sites. In their electrochemical and XPS study of arsenopyrite oxidation in an acid chloride medium (pH 1.5), Costa et al. (2002) also interpreted their data in terms of the formation of such diffusion-controlled overlayers.

Mikhlin and Tomashevich (2005) studied pristine and air-exposed natural arsenopyrite samples and material which had been subjected to oxidative leaching in acidified ferric chloride, sulfate and nitrate solutions. They recorded Fe *L*- , S *L*- and O *K*-edge XANES spectra. The data from air-exposed samples can be interpreted in terms of iron being initially mainly low-spin Fe^{2+} but with the growth of features associated with high spin Fe^{2+} and Fe^{3+}, the latter becoming predominant after lengthy exposure (1 week). This ferric iron is also interpreted as being associated with As species as reported by others including, as noted above, Schaufuss et al. (2000). Samples leached in the acid ferric chloride and sulfate solutions show spectra consistent with iron and arsenic-depleted, sulfur-enriched surface layers. In contrast, samples leached with acid ferric nitrate show a large concentration of surface Fe^{3+} species. Interesting observations are also made by these authors in regard to the changing electronic structure of the surface following such leaching reactions, and readers are referred to the original publication for further details.

Jones et al. (2003) studied acidic (pH 2.3) oxidative leaching of arsenopyrite in the presence of *Thiobacillus ferrooxidans* and the essential salts required to sustain bacterial growth. Reaction between arsenopyrite and *T. ferrooxidans* in the essential salts solution produced a uniform solid $FePO_4$ overlayer (~0.2 μm thick) within 1 week. The phosphate here is derived from the essential salts (no such layer was seen in a abiotic control experiment) and the layer continues to thicken with time, so that reaction continues with oxidation, diffusion, dissolution of arsenopyrite beneath the overlayer. The bacterial cells are separated from the arsenopyrite surface and it appears, therefore, that they do not need to be in contact with the arsenopyrite in order to promote rapid reaction.

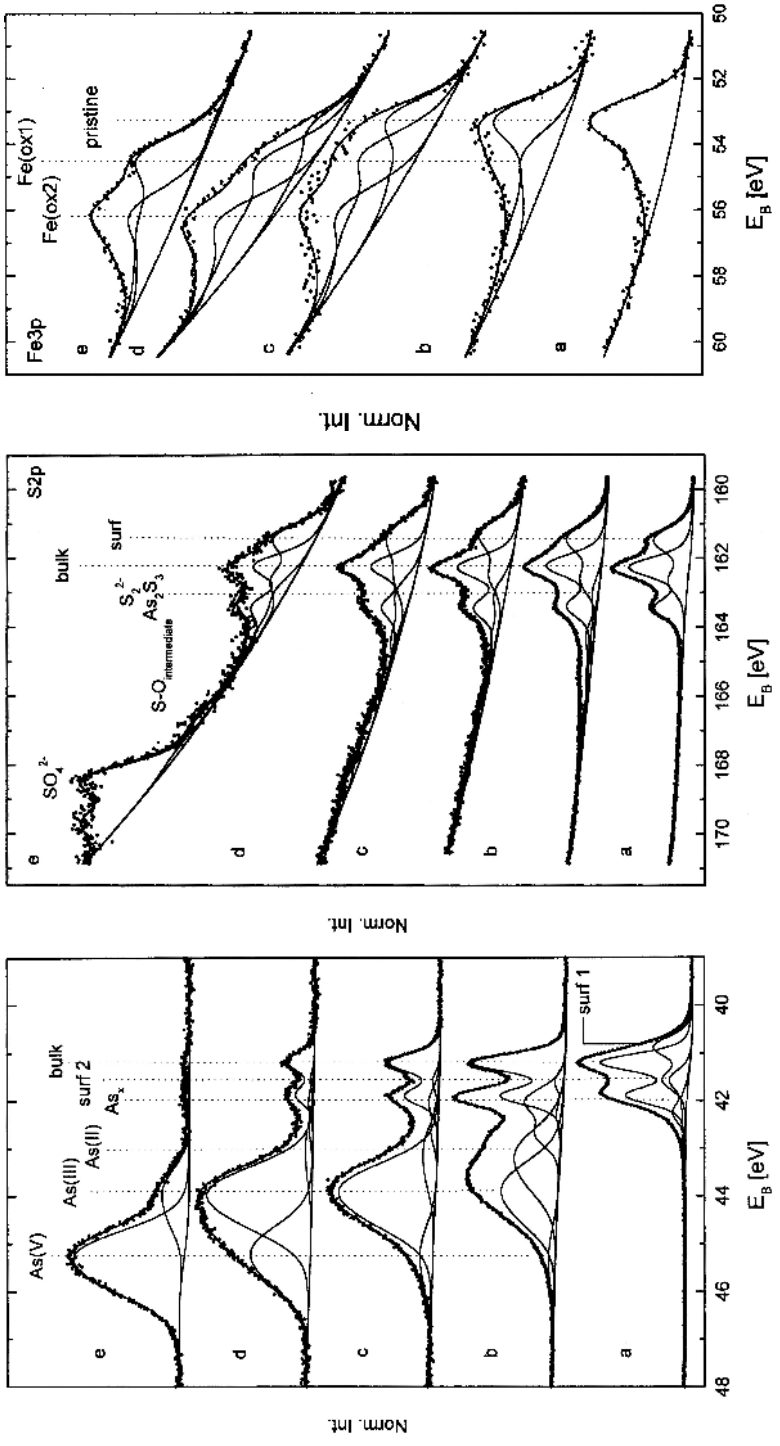

Figure 18. SR-XPS spectra of the As 3*d* (left), S 2*p* (center), and Fe 3*p* (right) regions for an arsenopyrite surface that is a) pristine and after exposure to b) 21,000 L O_2, c) 1 min air, d) 30 min air, and e) 22 hrs air. From Schaufuss et al. (2000).

CATALYSIS

There are very few known cases of true catalytic behavior for transition metal sulfide surfaces, where the surface itself is generally not altered or consumed in the chemical process. Therefore, it is of interest to examine the few cases where this behavior is known to occur. One such case is in hydrodesulfurization (HDS) reactions, which entails selective removal of organosulfur molecules from hydrocarbons produced from oil. Homogeneous HDS is accomplished by reacting these molecules with H_2 to cleave C-S bonds, forming H_2S and hydrocarbons as reaction products. RuS_2 is one of two naturally-occurring transition metal sulfides known to catalyze HDS reactions, the other being MoS_2. Other heteroatom removal reactions are also catalyzed by these surfaces, such as in hydrodenitrogenization. The heterogeneous HDS catalytic conditions are particularly aggressive, involving temperatures of about 600-700 K under a large excess of H_2 gas. Although the standard HDS catalytic material is currently MoS_2, RuS_2 surfaces are 13× more active for HDS of thiophene, a common HDS target molecule, than reference MoS_2 (Frechard and Sautet 1997a,b and references therein). Below, we review the studies of molecular-scale surface reactions underlying the HDS activity of these two materials. Because in both cases the active sites are predominantly believed to be undercoordinated metal atoms associated with sulfur vacancies, this review is also worthwhile as it is an excellent example of defect-driven surface chemistry, which is an important characteristic across the spectrum of possible surface chemical reactions occurring on transition metal sulfides and beyond.

Laurite

The adsorption of H_2 or H_2S gas on laurite (RuS_2) surfaces is relevant because ensuing reactions lead to changes in the surface stoichiometry and the creation of highly undercoordinated Ru. RuS_2 is a pyrite-type structure. As reviewed in the previous chapter (Rosso and Vaughan 2006), the (100) and (111) planes of RuS_2 are good cleavage surfaces involving primarily Ru-S bond rupture. The (100) surface is remarkably inert compared to other pyrite-type metal disulfides. The so-called activation step for preparing RuS_2 surfaces for HDS catalysis involves H_2 adsorption at high temperature to promote sulfur elimination and create coordinatively unsaturated Ru sites. These Ru sites are sufficiently electrophilic to react with electron density-donating organic molecules (Tan and Harris 1998).

The first step toward creating S vacancies is the surface hydrogenation step involving dissociative chemisorption of H_2 or H_2S to form surface -SH groups. The chemisorption of H_2 and H_2S on the stoichiometric RuS_2 (100) surface was modeled by Frechard and Sautet (1997a) using Hartree-Fock periodic slab calculations with post-self-consistent-field (SCF) DFT correlation energy corrections. They found that H_2 associatively (molecularly) chemisorbs preferentially to the 5-fold coordinated surface Ru atoms with a binding energy of 31 kcal mol^{-1}. The H_2 chemisorbs in a "side-on" bidentate configuration to single Ru sites (Fig. 19a). Although H_2 chemisorption at the Ru sites does not lead to dissociation, the H-H bond is greatly weakened by charge transfer from H_2 into p_z and d_{z^2} states of the underlying Ru atom. Dissociation of the H_2 to form Ru-H and an adjacent S-H is less energetically favorable (Fig. 19b,c) by 23 kcal mol^{-1} but is still more favorable than desorption of H_2. Formation of -SH groups only is energetically uphill relative to desorbed H_2, and this is due to the stability of the S_2 unit on this surface. H_2S molecules associatively chemisorb to single surface Ru sites with a binding energy of 35 kcal mol^{-1}. H_2S is electrostatically repelled from binding to surface S sites. As was the case for H_2 chemisorption, dissociation of H_2S at the surface producing Ru-SH and -SH groups is metastable. These observations led Frechard and Sautet (1997a) to conclude that S vacancy creation is likely to be initially slow on (100) terraces. Increasing numbers of these vacancies due to partial surface reduction is predicted to lead to favorable dissociative chemisorption because of enhanced unsaturated character at the Ru sites adjacent to those vacancies.

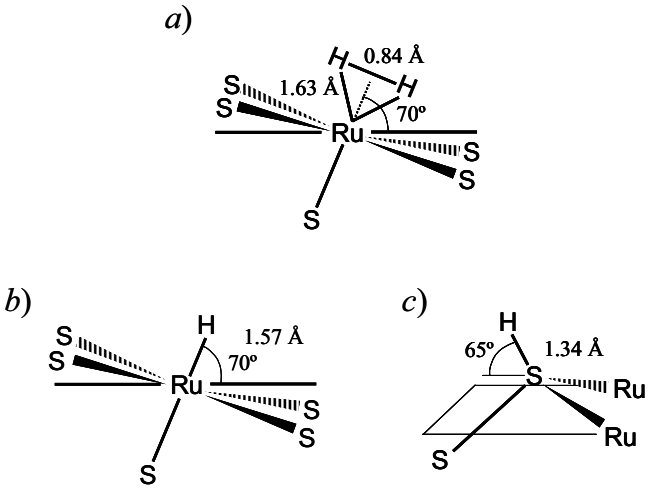

Figure 19. Schematics of the adsorption geometry of a) molecular H_2 and, after a dissociation step, separated hydrogen atoms on b) Ru and c) S surface sites, predicted from first principles calculations for the (100) RuS_2 surface. Redrawn after Frechard and Sautet (1997a).

On the RuS_2 (111) surface, the ability to hydrogenate the surface and create S vacancies is very different than for (100) because monosulfides are predicted which are more reactive with H_2 than S_2 dimers (Frechard and Sautet 1997b). The most stable structure of RuS_2 (111) in vacuum is not the charge neutral one, but rather a non-stoichiometric S-enriched one according to periodic Hartree-Fock calculations with post-SCF DFT, as well as according to planewave pseudopotential DFT calculations (Grillo and Sautet 2000) as reviewed in Rosso and Vaughan (2006). Dissociative chemisorption of H_2 is exothermic leading to a hydrogenated surface termination capped by three tilted –S-SH groups and one perpendicular –SH group. Further surface reduction is endothermic, proceeding through stages that involve decreasing the S:Ru ratio through S removal at protonated S_2 dimers by production of H_2S (costing 66 kcal mol^{-1}), followed by further S removal and the formation of -RuH metal hydride groups (costing an additional 180 kcal mol^{-1}) (Fig. 20). This yields the final (111) surface termination for use in HDS reactions, one which is significantly more catalytically active than the RuS_2 (100) surface.

Interaction of thiophene with hydrogenated and nonhydrogenated (100) and (111) RuS_2 surfaces has been recently modeled at the DFT level of theory (Smelyansky et al. 1998; Aray and Rodriguez 2001; Grillo and Sautet 2001; Aray et al. 2002, 2005). The sulfur atom of thiophene chemisorbs in a tilted η^1 configuration (in the language of organometallic chemistry; monodentate involving one atom in the heterocycle) to 5-fold surface Ru atoms on the stoichiometric nonhydrogenated (100) surface (Fig. 21). This monodentate Ru-S interaction (calculated E_{ads} = 0.43 eV for one thiophene on a 1×1 slab model, E_{ads} = 0.38 eV for one thiophene on a 2×1 supercell model) does not lead to distortions in the thiophene molecule towards cleavage of C-S bonds (Smelyansky et al. 1998). Reduction of the surface by cleaving the uppermost S_2 layer, leaving a 1:1 ratio of surface S vacancies and monosulfides, leads to an additional bond (Ru-C) formed between thiophene and another Ru atom of the surface, yielding a bridging η^2 configuration (Fig. 21). This interaction (E_{ads} = 0.1 eV) is weaker but involves distortion of the charge density distribution and geometry of the thiophene molecule consistent with activation of C-S bonds towards dissociation. The question arises whether hydrogenation of the surface is only important for creating S vacancies

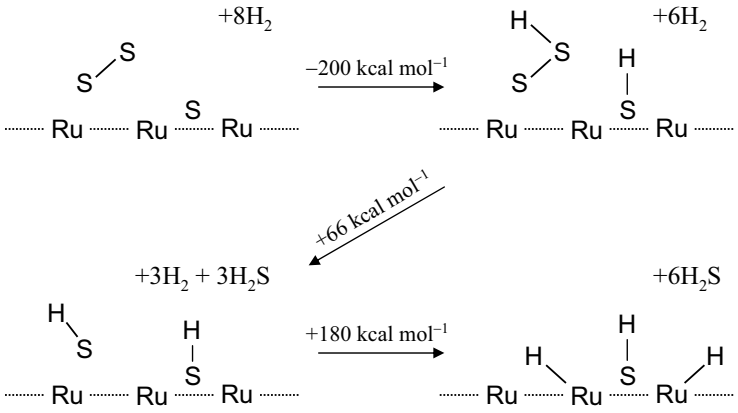

Figure 20. A model for the reduction of the RuS_2 (111) surface by molecular hydrogen, based on *ab initio* calculations. Redrawn after Frechard and Sautet (1997b).

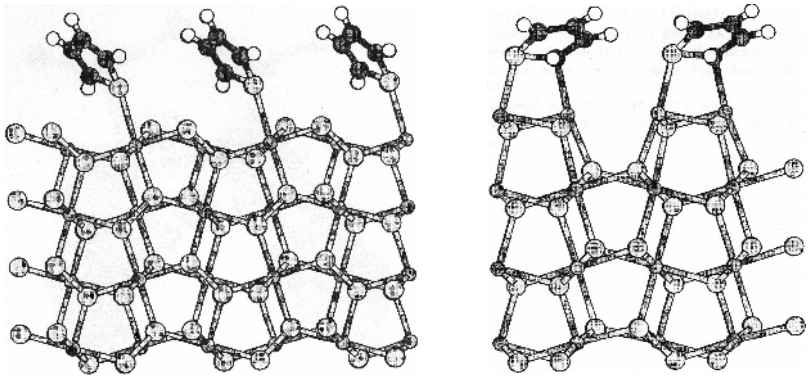

Figure 21. DFT-calculated adsorption geometries for thiophene on stoichiometric nonhydrogenated RuS_2 (100) surface (left) and the reduced RuS_2 (100) surface (right). [Used with permission of The American Physical Society from Smelyansky et al. (1998), *Physical Review B*, Vol. 58, Figs. 2 and 3, pp. R1783 and R1784.]

at the surface or does it also participate in C-S bond cleavage in thiophene? This question was addressed for a reduced (111) surface consisting of various ratios of -SH and -RuH groups using first principles calculations (Grillo and Sautet 2001). In that study, it was learned that the most favorable adsorption with respect to activation of C-S bonds involves a parallel thiophene η_2 configuration that is stabilized by interaction with the –RuH hydride groups at the surface. The role of H_2 therefore appears to be twofold, serving both to promote the formation of undercoordinated Ru by S abstraction and to destabilize C-S bonds by stronger thiophene hybridization to surface hydride groups.

Molybdenite

Considerably more work has been performed to understand the HDS catalytic activity of molybdenite (MoS_2) surfaces. As is the case for RuS_2, undercoordinated metal atoms are believed to be the catalytic sites for HDS reactions on MoS_2. Many of the concepts are the same, H_2 reacts with surface Mo and S sites, creating surface groups that lead to modification

of the S:Mo ratio under the catalytic conditions. An important difference between the two materials in this regard pertains to the structure of MoS_2, which is a hexagonal layered structure type, as reviewed in the previous chapter (Rosso and Vaughan 2006). In contrast to the basal (0001) surface, the hexagonal edge surfaces expose coordinatively unsaturated Mo and S atoms. The Mo-terminated $(10\bar{1}0)$ is comprised of 4-fold coordinated Mo atoms, and the S-terminated $(\bar{1}010)$ edge is comprised of 2-fold coordinated S atoms. Because of the importance of MoS_2 for HDS catalysis, substantial attention has been paid to the structure of the edge surface in equilibrium with H_2 and sulfur species such as H_2S, sulfhydryl groups, and sulfur-bearing organics (Raybaud et al. 1998; Helveg et al. 2000; Raybaud et al. 2000a,b; Schweiger et al. 2002; Travert et al. 2002; Paul and Payen 2003; Lauritsen et al. 2004a,b). The catalytic activity is known to be correlated with the S:Mo ratio along the edge surfaces, which in turn depends on the background partial pressure of sulfur. DFT studies of S addition to the Mo-edge and S removal from the S-edge under a fixed chemical potential of H_2 and H_2S have provided thermodynamic stability diagrams for edges with differing S:Mo ratios (Raybaud et al. 2000a; Schweiger et al. 2002). These are partly motivated by STM observations of variable MoS_2 nanoparticle morphologies depending on the H_2S:H_2 ratio during synthesis (Helveg et al. 2000; Lauritsen et al. 2004a). Synthesis in H_2S:H_2 = 500 is observed to yield a triangular morphology whereas synthesis in H_2S:H_2 = 0.07 yields a hexagonally truncated morphology (Fig. 22) (Lauritsen et al. 2004a). Raybaud et al. (2000a) used the so-called *ab initio* thermodynamics approach to examine edge structures treated with periodic boundary conditions. Schweiger et al. (2002) used the same approach with aperiodic cluster models to

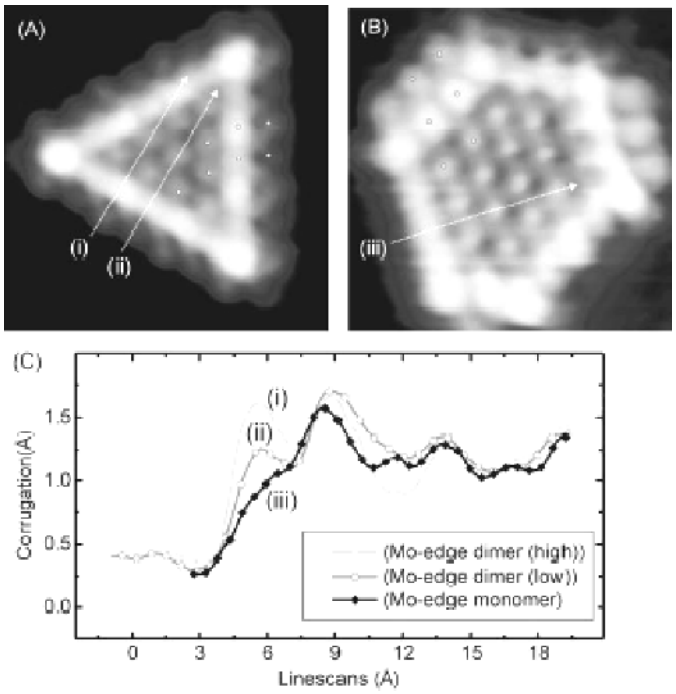

Figure 22. a) Atom-resolved STM image of a triangular single-layer MoS_2 nanocluster synthesized under "sulfiding conditions" (45×46 Å^2), and b) atom-resolved STM image of a hexagonal single-layer MoS_2 nanocluster synthesized under "sulfo-reductive" conditions (27 × 28 Å^2), and c) STM corrugation measurements across the Mo-edges of the triangle and hexagon. [Used with permission of Elsevier from Lauritsen et al. (2004a), *Journal of Catalysis*, Vol. 221, Fig. 2, p. 512.]

assess edge surface stability and the morphology of single-sheet triangular MoS_2 nanoparticles (for discussion of sulfide nanoparticles see also Pearce et al. 2006). In general, they use the grand canonical potential expression (Schweiger et al. 2002):

$$\Omega\left(n,\mu_S\right) = E_{MoS_x} - \mu_{Mo} n_{Mo}^{tot} - \mu_S n_S^{tot} \tag{16}$$

where E_{MoSx} is the DFT total energy of a triangular cluster of size n, and n_{Mo}^{tot} and n_S^{tot} are the total number of Mo and S atoms, respectively. At thermal equilibrium, the chemical potentials of S and Mo satisfy:

$$2\mu_S + \mu_{Mo} \approx E_{MoS_2}^{ref} \tag{17}$$

where $E_{MoS_2}^{ref}$ is the total energy of an infinite MoS_2 monolayer per MoS_2 unit, which gives:

$$\Omega\left(n,\mu_S\right) = E_{MoS_x} - n_{Mo}^{tot} E_{MoS_2}^{ref} - \mu_S\left(2n_{Mo}^{tot} - n_S^{tot}\right) \tag{18}$$

where n_S is the excess or lack of S atoms with respect to the MoS_2 stoichiometry. The chemical potential of S is related to the temperature and the partial sulfur pressure by simple thermodynamics as detailed in Raybaud et al. (2000a). The edge surface energy per surface site, $\sigma(\mu)$, is the slope of the grand canonical potential with respect to cluster size, i.e.:

$$d\Omega\left(\mu\right) = \sigma\left(\mu\right) dn \tag{19}$$

After accounting for the corner energies, the equilibrium morphology of a MoS_2 nanoparticle is determined using:

$$\frac{\sigma_{Mo}}{d_{Mo}} = \frac{\sigma_S}{d_S} \tag{20}$$

where σ's and refer to minima in the surface energies for the Mo and S edge types, and d's refer to distances from the Mo and S edges to the center of mass of the particle. Using this general strategy, Schweiger et al. (2002) were able to predict stable edge structures and nanoparticle morphologies for conditions relevant to HDS, concluding that the stable nanoparticles are deformed hexagons with 60% Mo-edge and 40% S-edge terminations (Fig. 23). They used this same approach to make structure/morphology predictions for the nanoparticles grown under a high partial pressure of H_2S for comparison with those grown for STM observations. This work also showed that S-vacancy formation is easier at the nanoparticle corners under HDS conditions, suggesting that the corner sites may have a higher catalytic activity than the edges. Collectively, this example demonstrates a great deal of utility in using *ab initio* thermodynamics for predicting changes in the structure of a mineral surface due to equilibration with another phase.

FUNCTIONALIZATION AND SELF-ASSEMBLY

In this section, we focus our attention on the chemical functionalization of sulfide mineral surfaces and on their ability to promote self-assembly of organic molecules. Surface functionalization is the introduction of new chemical functional groups to the surface by adsorption of molecules that bear the functional group of interest along with, typically, groups that specifically bind to the sulfide mineral. Functionalization is usually viewed as an intentional activity of the surface chemist performed with the aim of replacing the original chemical interface at the mineral surface (e.g., sulfide/water) with another interface (e.g., sulfide-O-CS_2/water) so as to impart new reactive behavior. Self-assembly is the process of spontaneous matter organization at the surface, usually mediated by a combination of specific adsorbate-surface and adsorbate-adsorbate interactions. It typically involves ordering in one (e.g., along a step) or

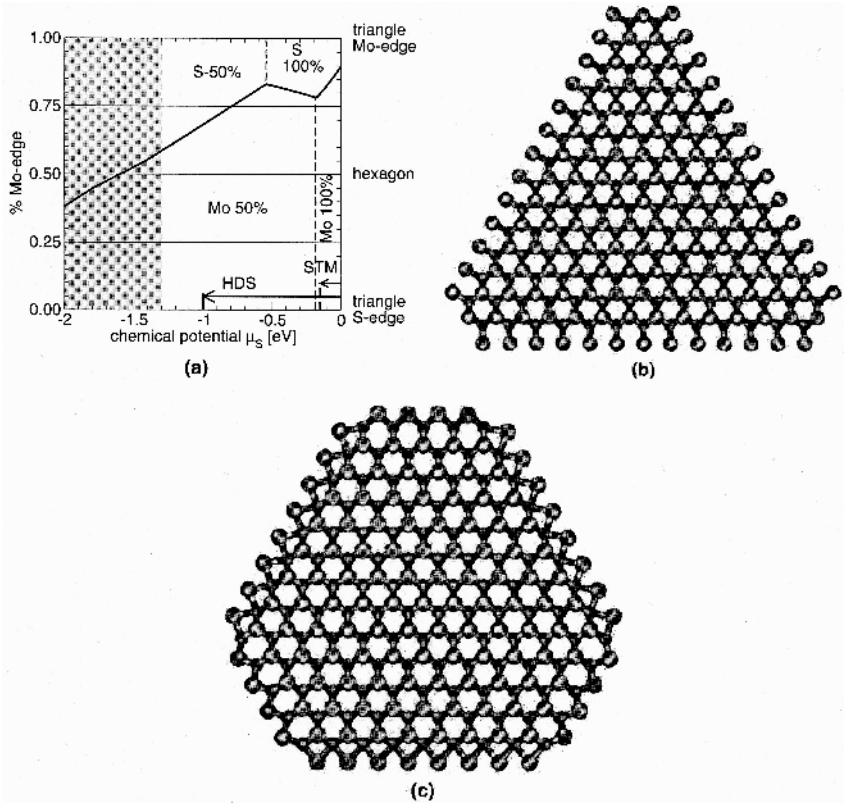

Figure 23. a) Morphology of nanosize MoS_2 particle as a function of the chemical potential of sulfur, based on *ab initio* thermodynamics calculations, and two predicted MoS_2 clusters for b) vacuum conditions during STM imaging, and c) hydrodesulfurization working conditions. [Used with permission of Elsevier from Schweiger et al. (2002), *Journal of Catalysis*, Vol. 207, Fig. 6, p. 83.]

two dimensions along the surface plane. Self-assembly is an important means of synthesizing molecular structures with higher order complexity that would otherwise never spontaneously form. Therefore it is viewed as a possible pathway for construction of, for example, polymeric nucleic acid sequences from monomeric amino acids in prebiotic Earth environments. Functionalization and self-assembly are not mutually exclusive processes; functionalizing adsorbates can also be self-assembled at the surface. Such is possibly the case for surfactant collector molecules as discussed below. Also, it is conceivable that functionalization could depend on self-assembly to attain the desired chemical behavior at the surface. The central theme of specific adsorption at the surface, typically of organic molecules, is an aspect of both of these processes that makes them more convenient to review together than apart.

Collector molecule adsorption

The majority of the work performed on sulfide mineral functionalization so far has been motivated by improving mineral separation technology. Although other applications are emerging, froth flotation is still the most important application for sulfide surface functionalization. Froth flotation is a chemical approach used in the mining industry for achieving mineral separation. A surfactant adsorbate (the collector molecule) is introduced to aqueous mixed-phase mineral suspensions to adsorb specifically to sulfide minerals, usually

by chelation of surface metal atoms. The adsorbed collector induces changes in the surface hydrophobicity to facilitate air bubble attachment and sulfide mineral separation into a stable froth. A major research goal is to understand adsorption mechanisms for various collector molecules to improve separation efficiency, selectivity, and to enable the next generation of tailored collector molecules to be developed.

Short chain-length thiol surfactants, such as xanthates (alkyl dithiocarbamates; R-O-CS_2), are regularly used as collector molecules. A number of studies have attempted to investigate the mechanistic details of ethylxanthate ($CH_3CH_2OCS_2^-$) and other xanthate anion adsorption onto various sulfide minerals (e.g., Allison et al. 1972; Leppinen and Rastas 1986, 1988, 1989; Ackerman et al. 1987; Leppinen et al. 1989; Nowak 1993; Valli et al. 1994; Valli and Persson 1994a,b; Voigt et al. 1994; Fornasiero et al. 1995; Mielczarski et al. 1995, 1996a,b,c,d, 1997, 1998; Kartio et al. 1999; Pattrick et al. 1999; Larsson et al. 2000; Porento and Hirva 2002, 2003, 2004, 2005; Hung et al. 2003, 2004). Much of the current state of knowledge in this area has been facilitated by vibrational spectroscopic analysis of adsorbate structures and surface speciation, such as by using Fourier transform infrared (FTIR) spectroscopy (sometimes) in the diffuse reflectance (DRIFT) configuration for *ex situ* measurements or the attenuated total reflectance (FTIR-ATR) configuration for *in situ* measurements. For example, Persson and co-workers used *ex situ* DRIFT spectroscopy and XPS to study ethylxanthate interaction with arsenopyrite, millerite, molybdenite, orpiment, and realgar (Valli et al. 1994), and covellite (Valli and Persson 1994a), and chalcopyrite, marcasite, pentlandite, pyrrhotite, and troilite (Valli and Persson 1994b). The experiments were performed on partly oxidized samples by exposing mineral powders made by grinding larger natural crystal specimens in air to ethylxanthate aqueous solutions. A summary of mechanistic findings for these and five other sulfide minerals was given in Valli et al. (1994) and are summarized in Table 1. In general, they found that the interaction could be dominated by: (1) ethylxanthate oxidation

Table 1. Observed surface products from the interaction of sulfide minerals and aqueous solutions of ethylxanthate (EtX = $CH_3CH_2OCS_2$) compared to products expected depending in part on a crystal chemical model for lattice sulfur oxidation potential based on S-S distances. Adapted from Valli et al. (1994).

Mineral	**Formula**	**Shortest S-S distance (Å)**	**Expected surface product**	**Observed surface product**
Acanthite	Ag_2S	4.135	Ag(I)EtX	Ag(I)EtX
Arsenopyrite	FeAsS	3.197	EtX_2	EtX_2, As(III)EtX_3
Chalcocite	Cu_2S	3.710	Cu(I)EtX	Cu(I)EtX
Chalcopyrite	$CuFeS_2$	3.685	Cu(I)EtX	Cu(I)EtX
Covellite	CuS	2.084, 3.757	Cu(I)EtX, EtX_2	Cu(I)EtX, EtX_2
Galena	PbS	4.194	Pb(II)EtX_2	Pb(II)EtX_2
Marcasite	FeS_2	2.223	EtX_2	EtX_2
Millerite	NiS	3.244	EtX_2	EtX_2
Molybdenite	MoS_2	3.154	EtX_2	EtX_2
Orpiment	As_2S_3	3.242	EtX_2	As(III)EtX_3, EtX_2
Pentlandite	$(Fe,Ni)_9S_8$	3.362	EtX_2	EtX_2
Pyrrhotite	$Fe_{1-x}S$	3.390	EtX_2	EtX_2
Pyrite	FeS_2	2.177	EtX_2	EtX_2
Realgar	AsS	3.295	EtX_2	EtX_2, As(III)EtX_3
Sphalerite	ZnS	3.821	Zn(II)-OCS_2	Zn(II)-OCS_2
Troilite	FeS	3.348	EtX_2	none

to dixanthogen by strongly oxidizing species present at the mineral surface such as $S_2O_7^{2-}$ or $S_2O_8^{2-}$; (2) formation of solid phase metal alkylxanthate salts by dissolution/re-precipitation, and (3) chemisorption of alkylxanthate species. The first two possibilities obscure information pertaining to the formation of alkylxanthate surface complexes. For example, for sulfides where Cu, As, or Pb is the metal atom, their surfaces tend to form the low solubility phases Cu(I)ethylxanthate, As(III)ethylxanthate, and Pb(II)ethylxanthate (Table 1). The relative amounts of $S_2O_x^{2-}$ species present at the surfaces leading in cases of $x > 6$ to the production of dixanthogen was postulated to depend ultimately on S-S distances in the structure, with shorter S-S distances tied to more production through more facile conversion to highly oxidizing $S_2O_x^{2-}$ species. Only in the cases of CdS (greenockite) and ZnS (sphalerite) were chemisorbed alkylxanthate surface complexes not obscured and positively identified (Valli et al. 1994).

The findings of these early studies were further clarified using similar FTIR spectroscopic methods for the minerals pyrrhotite (Fornasiero et al. 1995), chalcopyrite, tetrahedrite, and tennantite (Mielczarski et al. 1996c, 1997). Fornasiero et al. (1995) confirmed the formation of dixanthogen on pyrrhotite surfaces and proposed a model of sequential anion adsorption forming dixanthogen at surface sites. Mielczarski et al. (1996c) confirmed the formation of a cuprous xanthate complex on chalcopyrite surfaces and also found evidence for dixanthogen and the formation of Fe(OH)ethylxanthate due to partial oxidation of the initial chalcopyrite surface. Tetrahedrite and tennantite were found only to form the cuprous xanthate complex. Using a potentiostat controlled cell and a range of overpotentials from the open circuit potential (OCP) to ~200 mV higher than the OCP, Mielczarski et al. (1997) proposed four possible ethylxanthate adsorption mechanisms on chalcopyrite surfaces. These are the formation of dixanthogen according to:

$$EtX^- = 0.5EtX_2 + e^- \tag{21}$$

where EtX = $CH_3CH_2OCS_2$, the formation of iron hydroxyl xanthate complexes by the replacement reaction:

$$Fe(OH)_x + yEtX^- = Fe(OH)_{x-y}EtX_y + yOH^- \tag{22}$$

the formation of cuprous xanthate complex in the reaction:

$$CuFeS_2 + xEtX^- = Cu_{1-x}FeS_2 + xCuEtX + xe^- \tag{23}$$

and the formation of dixanthogen in the reaction:

$$Fe^{3+} + EtX^- = 0.5EtX_2 + Fe^{2+} \tag{24}$$

The availability of oxidized iron at the surface controls iron hydroxyl xanthate complex formation (Eqn. 22). In the case of fresh chalcopyrite surfaces where little or no oxidation has occurred, or for high $Cu:EtX^-$ concentration ratios at the surface, the formation of cuprous xanthate complexes is expected to dominate (Eqn. 23). For low $Cu:EtX^-$ concentration ratios, dixanthogen is produced at the surface. The degree of initial surface oxidation thus strongly influences the nature of the surface products and the degree with which the chalcopyrite surface is functionalized for hydrophobic flotation.

The importance of the metal-xanthate interactions for sulfide mineral flotation led to detailed molecular computational studies being performed. Porento and Hirva (2002) evaluated the energetics of bidentate complex formation between Cu^+, Cu^{2+}, Zn^{2+}, and Pb^{2+} and ethylxanthate, along with several other related prospective collector molecule designs using gas-phase *ab initio* calculations. The ethoxy tail (EtO, where Et = ethyl) adjacent to the thiol groups of the ethylxanthate molecule was systematically replaced with EtS, $EtCH_2$, EtNH, Et_2N, Et_2P, and $(EtO)_2P$ groups to examine the electronic effects on the interaction

energies. The types of metal complexes considered are shown in Figure 24, and corresponding complex formation energies (enthalpies under the usual assumption that $\Delta E \sim \Delta H$ where ΔE is the total electronic energy difference) calculated at the DFT level of theory on Hartree-Fock-optimized structures are listed in Table 2. This work showed that metal chelation by the thiol group is strongest for diethyldithiocarbamate anions (Et_2N), suggesting a possible new class of efficient collector molecules.

The success of correlating the behavior of monomeric metal-xanthate complexes to surface complexes is contingent upon factors not treated such as sulfide mineral surface structure and steric effects for collector adsorption. There have been several attempts to directly address this aspect. Using FTIR-ATR, Larsson et al. (2000) studied the adsorption of heptylxanthate on ZnS window elements with undetermined surface structure or crystallographic orientation. They found evidence for a predominantly biatomic bidentate "bridging" surface complex where the sulfur atoms of the xanthate CS_2 group bind to two separate Zn atoms. However, it is known that sphalerite does not float in acid or alkaline media with modest ethylxanthate concentration, possibly due to the high solubility of zinc ethylxanthate. The addition of Cu^{2+} effectively "activates" the sphalerite for flotation by forming copper sulfide on the sphalerite surface via $Cu \rightarrow Zn$ substitution and subsequently allowing strong copper ethylxanthate complexes to form. Pattrick et al. (1999) studied this system in detail at pH 10 and 12 using fluorescence reflection extended X-ray absorption fine-structure spectroscopy (REFLEXAFS). They found that Cu interacts with surface S atoms and in addition Cu-O bonds are formed.

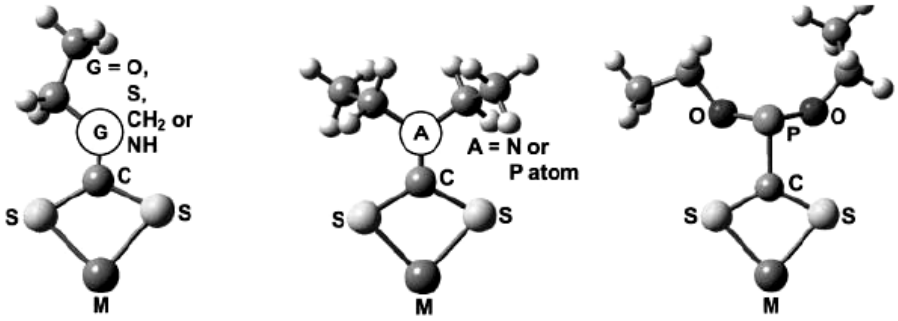

Figure 24. Chelate structure of metal ethyl thiol complexes (left), metal diethyl thiol complexes (center), and metal diethoxyphosphinecarbondithioic acid (right) used in the DFT study of Porento and Hirva (2002); (*M* = Cu, Zn, or Pb). [Used with permission of Springer-Verlag from Porento and Hirva (2002), *Theoretical Chemistry Accounts*, Vol. 107, Fig. 2, p. 203.]

Table 2. Complex formation energies (kJ/mol) for a range of collector anions and metal cations calculated at the DFT level of theory on HF-optimized structures. From Porento and Hirva (2002).

Collector	**Cu^+**	**Pb^{2+}**	**Zn^{2+}**	**Cu^{2+}**
Et_2N	−756	−1541	−1765	−1875
EtNH	−751	−1519	−1744	−1845
Et_2P	−704	−1461	−1696	−1785
EtO	−721	−1463	−1685	−1785
$EtCH_2$	−719	−1444	−1682	−1777
$(EtO)_2P$	−691	−1435	−1680	−1767
EtS	−699	−1443	−1670	−1763

S atoms of ethylxanthate were found to efficiently displace these oxygen atoms. The authors proposed a surface complex for ethylxanthate on the Cu-activated sphalerite surface that closely corresponds to covellite Cu-S surface species.

Porento and Hirva (2005) used *ab initio* electronic structure calculations on gas-phase cluster representations of sphalerite (111) with and without Cu substitution to examine mechanisms of forming metal-xanthate surface complexes. Given the focus on alkaline aqueous conditions, their treatment focused on ethylxanthate adsorption by a replacement reaction involving displacement of metal-bound surface hydroxyls. They found a strong correlation between the calculated energy for the replacement reaction and the location of Cu substitution sites in the cluster models (Fig. 25). The replacement reaction is more energetically favorable with hydroxyl bound to a surface Cu substitution site (which binds the hydroxyl less strongly

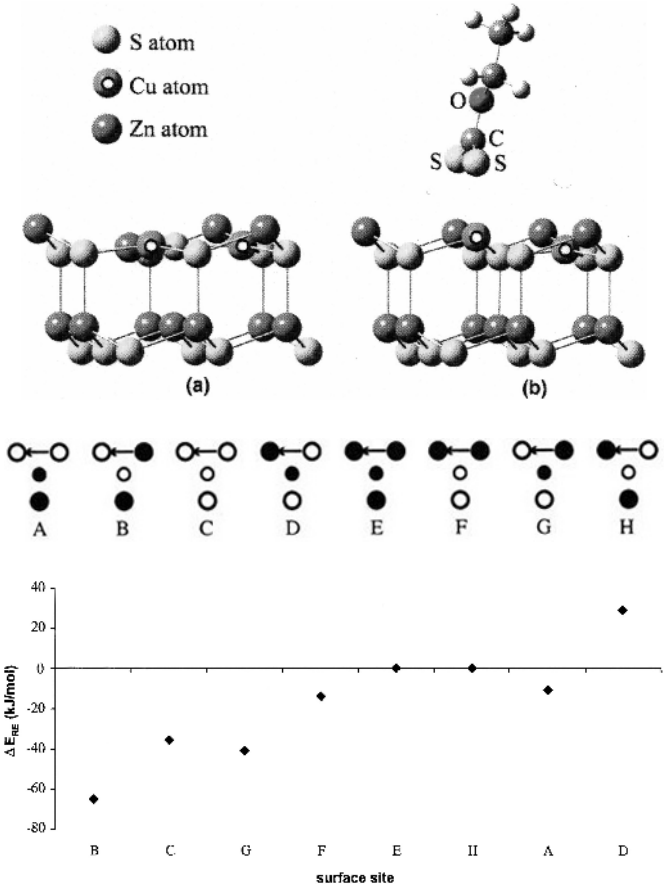

Figure 25. Findings of an *ab initio* calculation study of the influence of Cu substitution for Zn on ethylxanthate adsorption on the ZnS (111) surface. Structure models show example optimized cluster geometries for two Cu→Zn subsitutions a) before and b) after adsorption of ethylxanthate. The center diagram schematically shows the types of Cu-substituted configurations for the metal sublattice considered for co-adsorption energy calculations of OH^- and ethylxanthate, where open large circles are Cu atoms and closed large circles are Zn atoms, and the arrow points to the OH^- adsorption site and the orientation of the $-CS_2^-$ group. DFT-calculated energies for the various configurations are shown in the graph. [Used with permission of Elsevier from Porento and Hirva (2005), *Surface Science*, Vol. 576, Figs. 2, 4, and 5, pp. 101-103.]

than does a surface Zn site) and with a second Cu substitution present in the adjacent metal layer beneath. Consistent with Larsson et al. (2000), Porento and Hirva (2005) found that the CS_2 group of ethylxanthate binds to the surface by bridging two metal atoms. In an earlier *ab initio* study of the adsorption of ethylxanthate on covellite (001) in the gas-phase, Porento and Hirva (2004) also found that the bridging surface complex was the most stable configuration, in that case involving two surface Cu sites. Collectively these studies suggest that ethylxanthate adsorption onto Cu-activated sphalerite surfaces leading to facile flotation has crystal chemical ties to the structure of covellite.

Ethylxanthate adsorption has also been examined in detail for pyrite and galena. Hung et al. (2003) used planewave pseudopotential DFT to model the gas-phase adsorption of ethylxanthate and its head group moiety $HOCS_2^-$ on periodic slab representations of pyrite (110) and (111) surfaces. They found that $HOCS_2^-$ readily undergoes dissociation at 4-fold Fe sites present on the (110) surface (Fig. 26) and bridging S atoms on the (111) surface (see Rosso and Vaughan 2006). Because of structural similarities between these surface sites and defect sites expected in high densities on other pyrite surfaces, they concluded ethylxanthate would adsorb most strongly, by dissociative chemisorption, to defect sites where, for example, Fe coordination is four or less. In contrast to the bidentate bridging configuration discussed above for sphalerite and covellite, where metal-metal distances at the surface are a good match with the geometry of the xanthate head group, on pyrite (110) the tendency to dissociate may arise from the lack of ideal Fe-Fe distances at the surface. Given the previous discussion above on copper activation, it is noteworthy that pyrite flotation has also been observed to be enhanced by adsorption of copper, mechanisms for which have been examined by XPS (Voigt et al. 1994) and bear similarities to those discussed above for sphalerite (formation of stable copper ethylxanthate surface complexes).

Ethylxanthate adsorption onto galena surfaces has been examined by both macroscopic thermodynamic model fits to adsorption data based on vibrational spectroscopy (Leppinen and Rastas 1988; Nowak 1993), as well as being examined by SR-XPS (Kartio et al. 1999) and most recently by *ab initio* calculations at the DFT level of theory (Porento and Hirva 2003). Motivated by apparent discrepancies in the reported stabilities of surface lead xanthate on

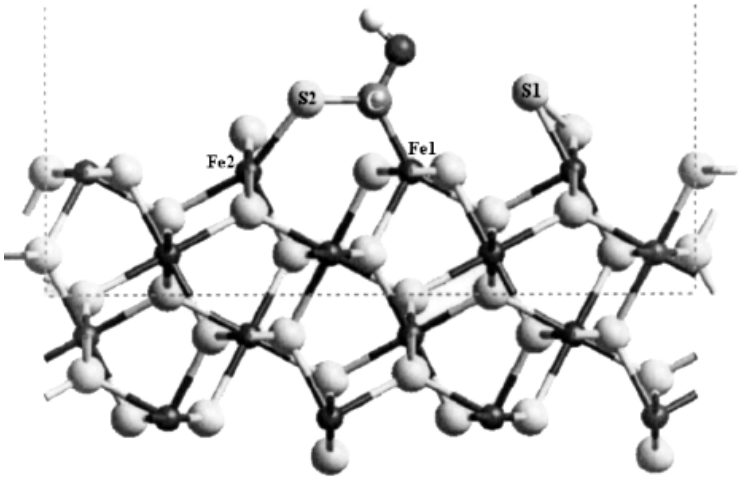

Figure 26. Calculated dissociative adsorption geometry for $HOCS_2^-$ on the FeS_2 (110) surface from DFT calculations. [Used with permission of the American Institute of Physics from Hung et al. (2003), *Journal of Chemical Physics*, Vol. 118, Fig. 2a, p. 6026.]

PbS versus precipitated lead xanthate, Leppinen and Rastas (1988) studied the chemisorption equilbria by analyzing the ethylxanthate and sulfide ion concentrations in the solution phase. It was found that the adsorption data cannot be explained using the thermodynamics of bulk PbS and Pb ethylxanthate phases. Therefore a mixed-phase model was invoked to describe the adsorption in terms of a combination of PbS and $(PbEtX)_2S$ species, written as:

$$2EtX^-_{(aq)} + 2PbS_{(sf)} \leftrightarrow (PbEtX)_2S_{(sf)} + S^{2-}_{(aq)} \quad (25)$$

where "sf" indicates "surface phase". The proposed equilibrium surface phase is characterized by partial surface coverage, as schematically shown in Figure 27. These findings figured heavily in the re-examination of this topic by Nowak (1993), who found in contrast that the adsorption data could be fit under the assumption of an adsorption density of one ethylxanthate molecule for every Pb surface site, and that the adsorption followed a Frumkin isotherm form. Using SR-XPS, Kartio et al. (1999) found that for freshly cleaved PbS exposure to 10^{-4} M ethylxanthate at pH 9.2, associated chemical shifts observed in the S 2*p* photospectra were consistent with the formation of chemisorbed xanthate ions at the surface, as opposed to the formation of bulk lead ethylxanthate (Fig. 28). The chosen exposure conditions had previously been shown by Buckley and Woods (1991) to produce near-monolayer coverage. In a detailed *ab initio* modeling study by Porento and Hirva (2003) at the DFT level using cluster representations of PbS (100), the stability of various possible ethylxanthate surface complex structures were compared (Fig. 29). In that study it was shown that an ethylxanthate molecule preferentially adsorbs as a monodentate complex over a surface Pb atom, where only one of the S atoms is bonded to a surface Pb atom. Collectively, this set of four studies provides a description of PbS functionalization by ethylxanthate that spans a range from the molecular to the macroscopic scales.

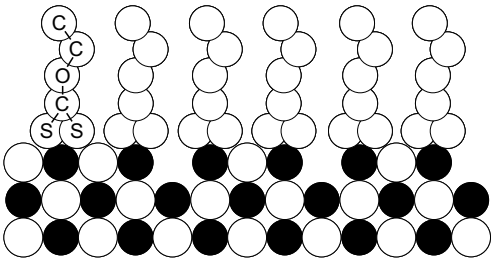

Figure 27. Suggested PbS (100) – ethylxanthate surface phase consisting of partial surface coverage from equilibrium thermodynamic calculations. Redrawn after Leppinen and Rastas (1988).

While the above discussion focused on ethylxanthate as the main example for sulfide surface functionalization, we note here that many other prospective collector molecules have also been studied. In particular, 2-mercaptobenzothiazole (MBT) has been regularly investigated alongside ethylxanthate since the 1980's. Adsorption mechanisms of MBT on a variety of sulfide minerals have been studied by electrophoresis and microcalorimetry (e.g., Maier and Dobias 1997), SR-XPS (e.g., Szargan et al. 1997), and ATR-FTIR (e.g., Larsson et al. 2001). The reader is referred to these articles and references therein for more information on MBT adsorption.

Self-assembly on sulfide mineral surfaces is a much more limited area of study. Relative to functionalization by collector molecule adsorption, the self-assembly research area can also be described as more exploratory. The molecules chosen for self-assembly studies on sulfide minerals so far have been selected primarily because of their general ability to form a self-assembled monolayer (SAM) on a range of materials. Collector molecule adsorption likely crosses over into this topic of self-assembly, because the collector molecules are surfactants which themselves have a tendency to self-assemble. This is a potentially important aspect of thiol collector molecule adsorption that has not been studied as such, possibly because of the specialized experimental techniques required to address molecular-orientation of sorbed species at surfaces. Other examples can be found where self-assembly was potentially relevant but not specifically addressed, such as in adsorption of 8-hydroxyquinoline (Lan et al. 2002) or

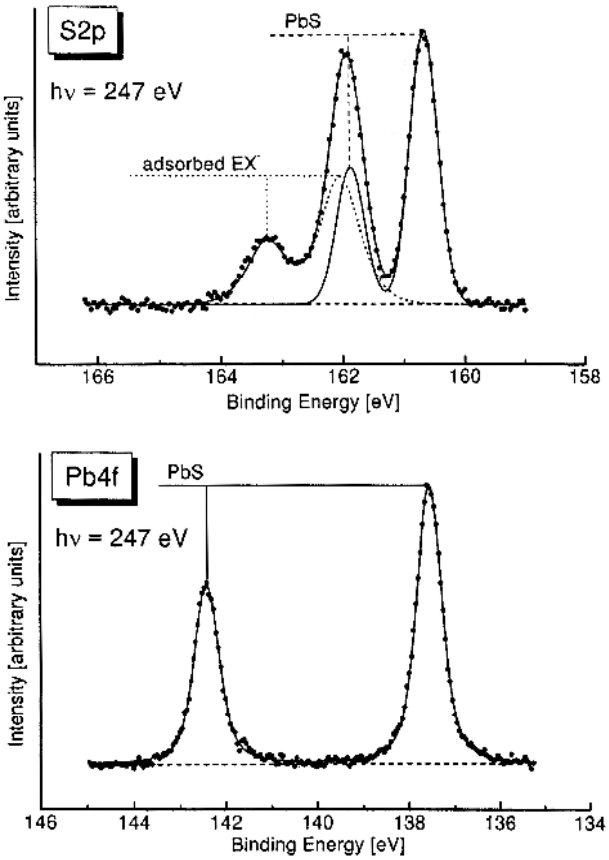

Figure 28. S 2*p* (top) and Pb 4*f* (bottom) SR-XPS spectra of PbS after immersion in 10^{-4} M potassium ethylxanthate solution (pH = 9.2) for 45 min. [Used with permission of Elsevier from Kartio et al. (1999), *Colloids and Surfaces A*, Vol. 154, Fig. 1, p. 99.]

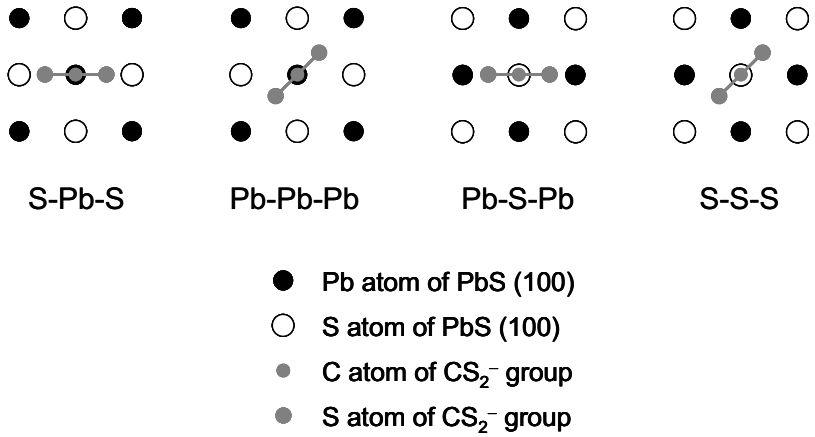

Figure 29. Various starting ethylxanthate adsorption configurations on PbS (100) tested in *ab initio* calculations on cluster models at the DFT level of theory. Redrawn after Porento and Hirva (2003).

L-α-phosphatidylcholine hydrogenated lipid and 1,2-*bis*-(10,12-tricosadiynoyl)-sn-glycero-3-phosphocholine lipid (Zhang et al. 2003) to pyrite surfaces (these studies were performed to investigate the formation of thin organic films as pyrite coatings to suppress oxidation). To our knowledge, self-assembly has so far only been specifically examined for pyrite and molybdenite surfaces. We review some of this work below.

The potential for self-assembly of triphenylphosphine, *n*-alkanethiols and *n*-alkylamines on pyrite was examined using XPS, IR spectroscopy, and near-edge X-ray absorption fine structure (NEXAFS) spectroscopy by Himmel et al. (1996). The pyrite was fractured approximately along the (100) plane, polished to 250 nm grit size, and chemically etched to remove oxidation products. XPS showed that the prepared surface was as free of oxidation products as pyrite fractured in inert Ar atmosphere. The authors found that *n*-alkylamines and triphenylphosphine adsorb to the pyrite surface and form dense monolayers. The *n*-alklyamines also displayed a high degree of orientation, with the alkyl chains oriented at a 25° average angle with respect to the surface normal. This is the first known example of a highly oriented molecular film formed on pyrite. The *n*-alkanethiol, which normally forms well defined monolayers on metal substrates, did not adsorb. Molecular modeling has also been used to simulate the formation of self-assembled layers on pyrite. Using MD simulations, Zhang et al. (2005) investigated self-assembly of dilithium phthalocyanine on the pyrite (100) surface. They found a strong dependence of the molecular orientation on packing density, with a preferred stacking axis perpendicular to the surface plane due to strong interactions between Li and surface S atoms.

Molybdenite (0001) surfaces offer the prospect of very flat ordered molecular layers to be formed. The structure of this surface is reviewed in the previous chapter (Rosso and Vaughan 2006). A wide range of organic adsorbates have been examined for their self-assembled film structure on MoS_2 (0001) including metal phthalocyanine (Ludwig et al. 1994; Strohmaier et al. 1996a), naphthalene-1,4,5,8-tetracarboxylic-dianhydride (Strohmaier et al. 1996b), and 4,4′,7,7′-tetrachloro-thioindigo (Petersen et al. 1997) for example. But these and many other studies were performed in vacuum chambers using such techniques as molecular beam epitaxy. Here we focus on the studies performed directly in solution because of their more direct relevance to the natural environment. Highly ordered herringbone-structure monolayers of dotriacontane ($C_{32}H_{66}$) were shown to form on this surface (although primarily on the close analogue phase, $MoSe_2$) using *in situ* STM to directly image the molecular structure of the films in solution (Cincotti and Rabe 1993). The adsorbate lattice is close-packed and oriented relative to the (0001) surface lattice but not simply commensurate. The self-assembly is attributed more to the atomic flatness of the surface and less to specific interactions between the dotriacontane molecules and the surface atoms.

In another set of in situ STM experiments, the influence of the surface lattice on the ordering of self-assembled films was specifically addressed by Giancarlo et al. (1998). They investigated the film structure on MoS_2 (0001) for a series of mono- and disubstituted long-chain hydrocarbons containing –S–, OH, COOH, Br, C=C, and $CONH_2$ functionalities. Specifically, they examined films of octadecyl sulfide, elaidic acid, 12-bromododecanoic acid, 12-bromododecanol, 11-bromoundecanol, octadecanamide. A diverse array of ordering patterns were observed with *in situ* STM; substantial attention was paid to assessing the electronic structure aspects of both the substrate and the film contributing to image contrast by bias dependent imaging (Fig. 30). They compared the ordering patterns obtained on MoS_2 (0001), where the surface lattice repeat is 3.2 Å, with those for the same molecules adsorbed onto graphite basal planes, where the surface lattice repeat is 2.5 Å. Three types of substrate influence on molecular ordering behavior were categorized; from those where there was no detectable influence, to slight influence involving substrate control on the size of ordered molecular domains, to a complete change in molecular ordering induced by the substrate (Table 3). Primary factors contributing to the differences in

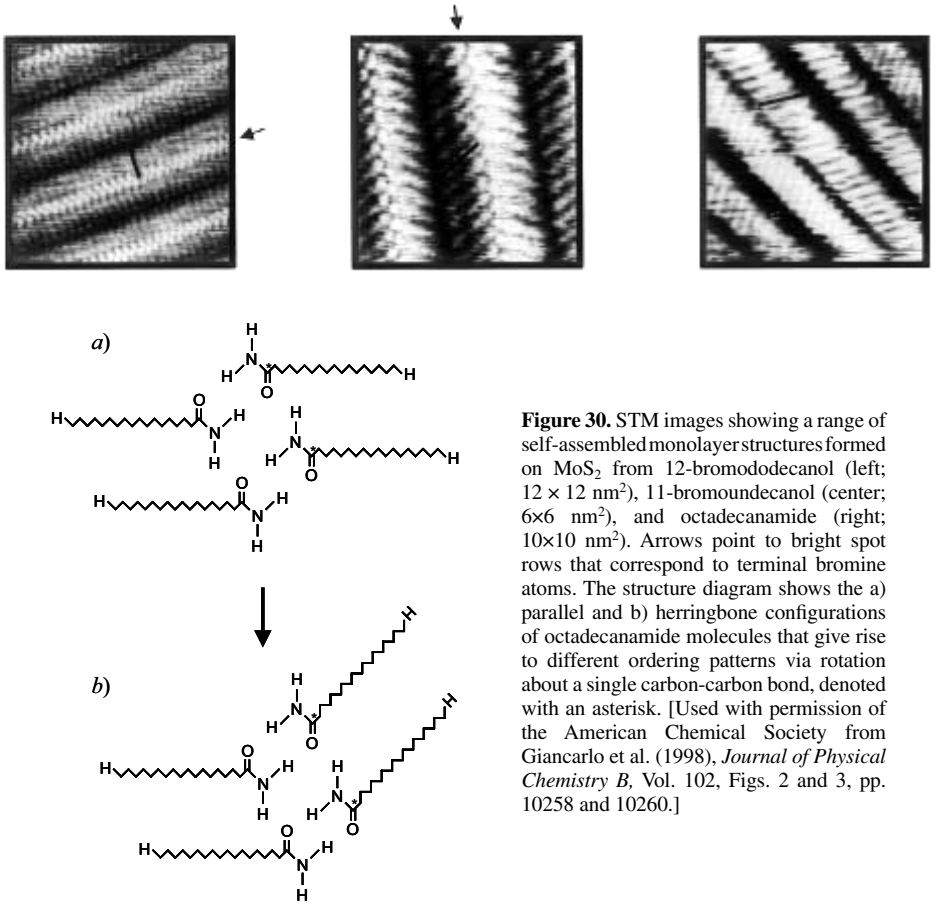

Figure 30. STM images showing a range of self-assembled monolayer structures formed on MoS_2 from 12-bromododecanol (left; 12×12 nm^2), 11-bromoundecanol (center; 6×6 nm^2), and octadecanamide (right; 10×10 nm^2). Arrows point to bright spot rows that correspond to terminal bromine atoms. The structure diagram shows the a) parallel and b) herringbone configurations of octadecanamide molecules that give rise to different ordering patterns via rotation about a single carbon-carbon bond, denoted with an asterisk. [Used with permission of the American Chemical Society from Giancarlo et al. (1998), *Journal of Physical Chemistry B,* Vol. 102, Figs. 2 and 3, pp. 10258 and 10260.]

Table 3. Comparison between molecular structure parameters and ordering behavior observed by STM for self-assembled thin films on MoS_2 compared to graphite (Giancarlo et al. 1998 and references therein). Molecular length is defined as the length of two molecules comprising a dimer pair.

Observed dependence on substrate	Molecule[a]	MoS_2 (0001)			Graphite (0001)		
		Molec. length (nm)	Angle (deg.)	Spacing between molec. (nm)	Molec. length (nm)	Angle (deg.)	Spacing between molec. (nm)
None	OS	4.38	90	0.48	4.35	99	0.43
None	EA	2.55	94	0.53	2.43	87	0.43
Slight	12-BA	3.24	115	—	3.70	117	0.42
Significant	12-B	1.86	93	0.45	1.78	—	0.46
None	11-B	1.43	56	0.41	1.51	63	0.49
Significant	O	2.37	117	0.47	2.4-2.6	115-120	0.48

[a]OS = octadecyl sulfide, EA = elaidic acid, 12-BA = 12-bromododecanoic acid, 12-B = 12-bromododecanol, 11-B = 11-bromoundecanol, O = octadecanamide.

behavior include the degree of molecular size-dependent registry between the packed organic film and the substrate repeat unit size, and the strength of adsorbate-substrate and adsorbate-adsorbate interactions, particularly intermolecular hydrogen bonding.

A rapidly growing component of self-assembly studies on mineral surfaces is focused on exploring the potential of this process to construct the biochemical machinery of life. For example, purine-pyrimidine arrays assembled on naturally occurring mineral surfaces might act as possible templates for biomolecular assembly. A number of studies have been performed to examine the monolayer formation mechanisms and structure of purine and pyrimidine bases on MoS_2 (0001), particularly those by Sowerby and co-workers (e.g., Sowerby et al. 1996, 1998a,b; Sowerby and Petersen 1999). Sowerby et al. (1996; 1998b) used STM to investigate the two-dimensional self-assembled monolayer structure for the purine base, adenine ($C_5H_5N_5$), on MoS_2 (0001). The molecules were observed to lie flat on the surface. Although formed from achiral adenine molecules, the observed adsorbate structures were enantiomorphic on molybdenite (Fig. 31). This phenomenon suggests a mechanism for the introduction of a localized chiral symmetry break, and it was concluded that the spontaneous crystallization of these molecules on inorganic surfaces may have some role in the origin of biomolecular optical asymmetry. Molecular mechanics calculations were used to identify possible organizations of the adenine monolayer on the MoS_2 (0001) surface and to determine its registry with the underlying surface atoms. A range of trial mesh and trial packing configurations were evaluated to determine those that are the most energetically stable. The optimal calculated structure involves a rectangular adenine repeat unit at an oblique angle with respect to the substrate lattice vectors. Molecular mechanics calculations were further applied to both adenine and guanine ($C_5H_5N_5O$) adsorption on MoS_2 (0001) and on the graphite basal plane (Sowerby et al. 1998a). The authors found that both self-assembled monolayer structures are similar to each other, adopting a *P*2gg plane group motif, independent of the structural differences between the two substrates. Central to the adsorbate structures is the formation of centrosymmetric dimers, which neutralizes strong dipole moments intrinsic to the individual

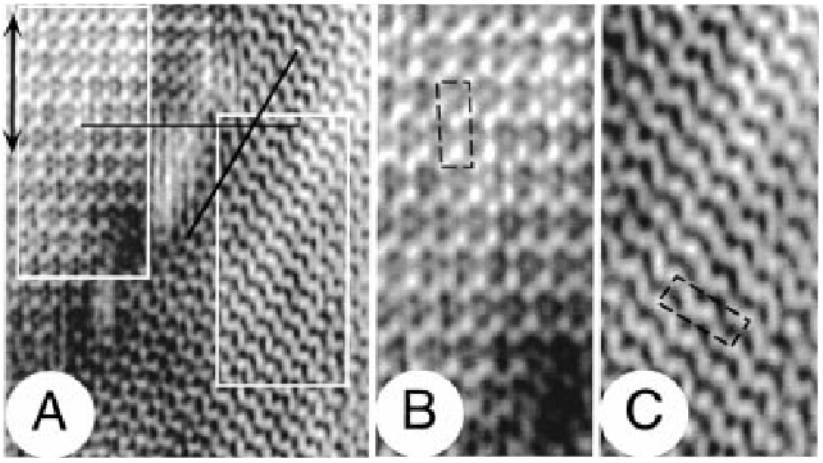

Figure 31. a) STM image of an ordered array of adenine molecules adsorbed to the surface of MoS_2 showing a grain boundary between two domains. Equivalent lattice directions on each of the domains are indicated by the black lines and intersect at an angle of 60°, indicating epitaxial registration with the underlying substrate. b,c) Enlarged portions of each of the domains in a) delineated by the white rectangles. On each image, the adsorbate mesh is described by the black dashed line parallelograms of dimensions 2.28×0.84 nm. [Used with permission of the American Chemical Society from Sowerby et al. (1998b), *Langmuir*, Vol. 14, Fig. 1, p. 5197.]

molecules. Finally, they noted that π-bond cooperativity, which contributes to the stability of cyclic hydrogen bonds between complementary base pairs in nucleic acids, requires that adjacent hydrogen-bonding functional groups to be linked by bonds with π-electron character. This condition is satisfied in the adenine and guanine self-assembled monolayers on MoS_2 (0001).

METAL ION UPTAKE

The uptake of metal ions at the surfaces of sulfide minerals is an important area of study. In nature, it is relevant to understanding the transport and mobility of metals in the Earth's crust and in surface and near-surface environments. Such understanding has applications to processes of importance in ore formation, and in the mobility of pollutants from mine wastes, industrial operations and other sources. Many metals are toxic to life forms, even at low concentrations. Metal uptake processes are also technologically important, for example in mineral extraction.

In highly controlled UHV experimental systems as discussed above, techniques such as XPS and STM can sometimes be used to probe the interaction of individual (gas phase) metal ions with carefully prepared sulfide surfaces. Such studies can provide insights into molecular scale interaction processes. A more direct interest, however, is in the interaction of metal ions in aqueous solution with sulfide mineral surfaces. These interactions can be investigated by performing experiments where sulfides are exposed to metal-containing solutions *ex situ* before transfer into UHV for surface analysis, or by using methods that do not require UHV conditions and where *in situ* analysis of the system is possible.

The uptake of metal ions in solution by mineral surfaces can involve one or more of a number of processes (Fig. 32). The metal ion may retain its hydration sphere and be weakly held to the surface as an *outer sphere complex* (effectively "physisorbed"). It may lose some of its hydration sphere and bond directly and more strongly to the surface as an *inner sphere complex* (effectively "chemisorbed"). It may replace ions at the surface (or even diffuse some distance into the solid) in an exchange reaction, or a more extensive reaction (possibly a redox reaction) with the surface may result in precipitation or co-precipitation of a new phase at the surface and/or wholesale replacement of the substrate.

Galena

Given its simple structure and perfect cleavage, it is not surprising that the uptake of metal ions by galena has been studied both experimentally and computationally. An area of particular interest has been uptake of gold and silver from aqueous solution by galena; here, surface reactions have been suggested as important in ore deposit formation, and also in the control of heavy metal concentrations in reducing aqueous environments. There is now an extensive literature dealing with experimental studies of such interactions with a variety of sulfides, but particularly galena and pyrite. Earlier studies using XPS, AES and (analytical) SEM to characterize surface species have been reviewed by Bancroft and Hyland (1990). These were followed by further investigations using the same range of techniques, in some cases supplemented with electrochemical methods or other spectrometries (Mycroft et al. 1995a; Scaini et al. 1995, 1997). New insights into the molecular scale nature of these interactions were made possible with the application of STM (Eggleston and Hochella 1991, 1993) and of quantum mechanical calculations aimed at exploring the energetics of the processes and simulating STM images, XPS and STS spectra (Becker et al. 1997). Experimental and computational evidence for uptake from solution of species such as $AuCl_4^-$, points to initial adsorption (as an inner sphere complex) at galena surface sites, followed by electron transfer and reduction of Au^{3+} to Au^0 with loss of ligands. This process is calculated

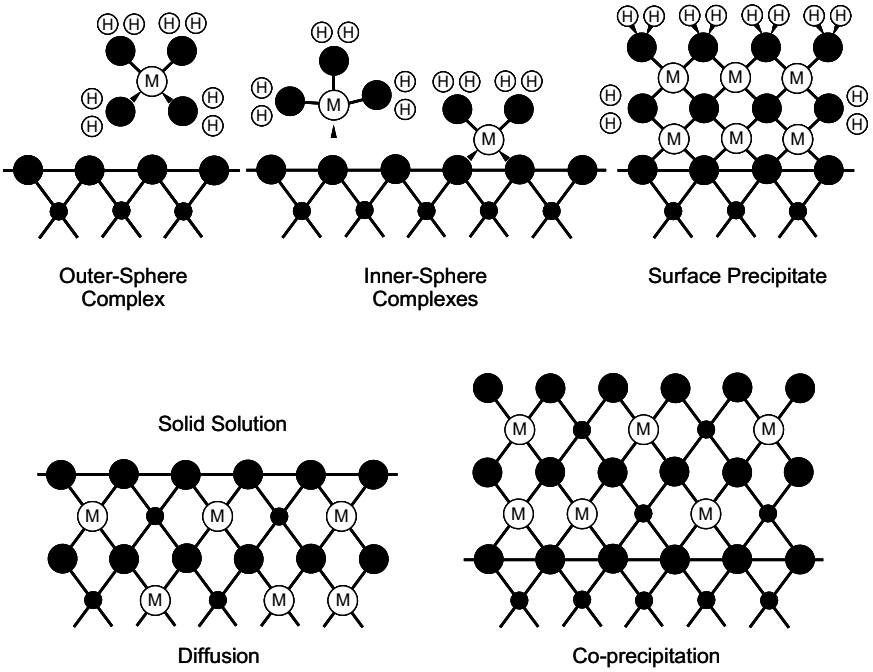

Figure 32. Depiction of various processes of metal ion uptake by mineral surfaces.

to be energetically favorable (Becker et al. 1997) which helps to explain the affinity of gold for surfaces of sulfides such as galena. The Au^0 is then stabilized at the surface by formation of Au-Au bonds to give dimers and islands of the metal.

In two other very different studies of the PbS (100) surface, Kendelewicz et al. (1998) used X-ray standing wave (XSW) and photoemission methods to study interaction with vapor-deposited sodium overlayers, and Genin et al. (2001) used XPS, XAS and reflection high energy electron diffraction (RHEED) to study interaction with mercury vapor. The former was a fundamental study of relaxation effects at the surface and of the possible influence of Na on surface reactivity. There is clear evidence of replacement of surface Pb^{2+} ions by Na^+, and the suggestion made is that local charge balance is achieved by having additional Na atoms atop S atoms at the surface. No evidence was found for enhanced reactivity to water, which does not react significantly with the flat PbS (100) surface (see discussion above). In the latter study, Hg^0 was seen to be reduced at the surface to Hg^{2+} and to be adsorbed through the formation of Hg-S bonds. Analysis of XAS data gave a Hg-S bond length of 2.62 Å and a structural model was suggested with Hg atoms adsorbed at 2-coordinate surface sites. At saturation, the adsorbed mercury was estimated to comprise a single monolayer covering the galena surface.

Pyrite

Pyrite, being by far the most abundant natural sulfide mineral, has been the subject of numerous studies of surface interaction with metal ions in solution. For example, a substantial body of work on uptake of precious metals, already referred to above, has been produced. As noted in sections of this and the preceding chapter, much spectroscopic and imaging work on pyrite surfaces has been undertaken to clarify the nature of the pristine surface and the surface reactions involved in pyrite oxidation and breakdown. It has been noted that unsaturated

surface groups can form that may react with water (Rosso et al. 1999b), and highly reactive defect sites may occur, partially stabilized by disproportionation (Guevremont et al. 1997; Uhlig et al. 2001). It appears that defect structures can serve as centers for electron transfer and promote disproportionation and cation uptake. For example, the adsorption of Ag^+ on pyrite probably involves sulfur disproportionation and electron transfer (Scaini et al. 1995):

$$FeS_2 + 8Ag^+ + 4H_2O \leftrightarrow Fe^{2+} + Ag_2S + 6Ag^0 + SO_4^{2-} + 8H^+ \quad (26)$$

The work on precious metal uptake has included studies of Au, Ag and Pd (see review by Bancroft and Hyland 1990) and explored interactions, with gold in particular, in several different oxidation states (Au^{3+}, Au^+) and different solution complexes (chloride, bisulfide). Other variables investigated have included pH and temperature. For example, in uptake of silver as chloride species by pyrite (and galena), changes in metal and chloride concentrations have a significant influence, but not pH variations (Scaini et al. 1997). Reactions of Au^+ bisulfide complexes with pyrite increase at elevated temperature (90 °C vs. 25 °C) and higher pH (6 vs. 3), but far less Au is deposited than from $AuCl^-$ solutions because of the greater stability of $Au(SH)_x^{1-x}$ complexes (Scaini et al. 1998).

The uptake from solution of a range of transition metals and heavy metals by the pyrite surface has also been studied. For example, Parkman et al. (1999) used bulk measurements of uptake as a function of initial concentration combined with X-ray absorption spectroscopy (EXAFS and XANES) to study reactions with Cu^{2+} and Cd^{2+} ions in solution at circum-neutral pH. In these experiments, the bulk uptake of Cd contrasts with that of Cu. The Cd shows decreasing efficiency of uptake with increasing concentration, and the Cu shows constant uptake which is an order of magnitude greater than for Cd. The behavior of Cu is attributed to formation (by precipitation/replacement) of a copper sulfide (of chalcocite or covellite type) at the surface, and this is in line with spectroscopic data showing bonding of Cu to an average of four sulfur atoms at 2.3 Å. The spectroscopic data for Cd indicates bonding to six oxygens at 2.28 Å over all measured concentrations. Combined with the bulk uptake behavior which suggests limited availability of surface sites for "sorption," the simplest interpretation of these data are outer sphere surface complexation. However, Parkman et al. (1999) suggest this is unlikely given the high capacity and relatively strong binding of Cd at low concentrations. The possibility of a more complex interaction process involving oxidation is suggested. Further clarification has come from a study by Bostick et al. (2000) using a range of methods including Raman spectroscopy, electron microscopy and STM. Here, complex reactions involving pyrite surface reconstruction and disproportionation are proposed, leading to a mixture of sulfide and oxide surface products (elemental sulfur, iron hydroxide and CdS).

Other studies of metal uptake by pyrite include investigations of Ni^{2+} (Hacquard et al. 1999), Hg^{2+} (Ehrhardt et al. 2000), As^{3+} and As^{4+} (Farquhar et al. 2002; Bostick and Fendorf 2003) and Mo^{6+} (Bostick et al. 2003). The work on Ni^{2+} "adsorption" was undertaken at pH 10 under conditions where "the mineral surface is rapidly covered by a layer of Fe^{3+} oxides". The first step of the interaction with nickel is then the formation of a hydroxylated surface complex (Hacquard et al. 1999). The "sorption" of Hg^{2+} was investigated as a function of pH and using XPS for analysis of pyrite surfaces exposed to the metal (Ehrhardt et al. 2000). The surfaces studied showed partial oxidation, with islands of Fe^{3+} oxyhydroxides as well as pyrite present. The XPS measurements were interpreted in terms of (inner sphere) surface complexation involving both pyritic functional groups and hydroxyl groups on the oxyhydroxide islands. No evidence was found for the formation of Hg sulfide, sulfate or thiosulfate.

Arsenic and molybdenum are species of particular interest in regard to surface uptake, the former because of its toxicity and the latter because of its importance as a nutrient needed for a variety of biological functions. Farquhar et al. (2002) used EXAFS and XANES to study the mechanisms of uptake of both As^{3+} and As^{5+} from aqueous solution at pH 5.5-6.5.

For both species, the primary coordination of arsenic sorbed at the pyrite surface was to four oxygen atoms (with As-O distances of 1.69 Å for As^{5+} and 1.73 Å for As^{3+} in line with expected trends). Evidence for Fe atoms at 3.35-3.40 Å lends further weight to the argument that both aresenite and arsenate species form outer sphere complexes at the pyrite surface under the conditions studied (Farquhar et al. 2002). In a study of arsenite sorption onto pyrite, Bostick and Fendorf (2003) using bulk sorption measurements, X-ray absorption spectroscopy and XPS, showed patterns of uptake that generally follow the Langmuir isotherms characteristic of interaction with a limited number of surface sites which eventually become saturated (monolayer capacity). Such behavior is in accord with the surface complexation suggested above. However, the spectra reported in this work have been interpreted in terms of formation of an "FeAsS-like surface precipitate." These discrepancies could arise from differences in starting materials and sample handling, although another explanation could be that Farquhar et al. (2002) worked at acid pH, where Bostick and Fendorf (2003) found lower sorption levels and closer adherence to Langmuir isotherm uptake behavior as a function of concentration.

Mo^{6+} uptake on pyrite, both as molybdate (MoO_4^{2-}) and as tetrathiomolybdate (MoS_4^{2-}), was studied by Bostick et al. (2003) using bulk sorption experiments and X-ray absorption spectroscopy. Both forms of Mo partition strongly on to pyrite under a wide range of pH and ionic strength conditions, although molybdate is readily desorbed whereas MoS_4^{2-} is retained even at high pH. The spectroscopic data were interpreted in terms of molybdate forming a bidentate, mononuclear complex on FeS_2 and tetrathiomolybdate forming Mo-Fe-S cubane-type clusters, consistent with its high affinity and resistance to desorption. Structural models for these surface complexes are shown in Figure 33.

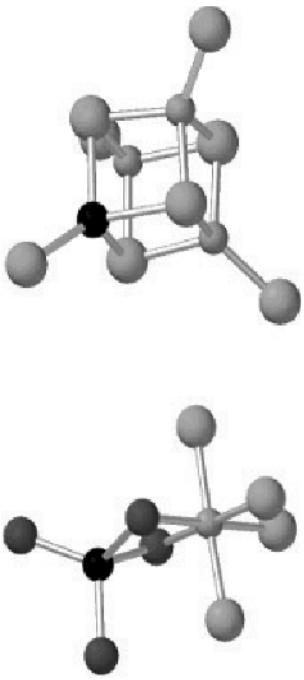

Figure 33. Structural models of (top) MoS_4^{2-} and (bottom) MoO_4^{2-} adsorption on FeS_2. Molybdate forms a bidentate, mononuclear complex with an Fe polyhedron, and MoS_4^{2-} forms a Mo-Fe-S cubane structure. [Used with permission of the American Chemical Society from Bostick and Fendorf (2003), *Environmental Science and Technology*, Vol. 37, Fig. 7, p. 290.]

Pyrrhotite and troilite

Very few studies of the uptake of metals by the surface of pyrrhotite have so far been undertaken. Given the relative complexity of this sulfide, this is not surprising. In a study which further explored the interaction of gold in solution with sulfide surfaces, Widler and Seward (2002) used potentiometric titrations, bulk measurements of uptake, and XPS to examine uptake of gold from Au(I) hydrosulfide solution complexes by pyrrhotite produced by hydrothermal synthesis. Under the conditions of these experiments, the mineral surface is negatively charged from pH 2 to pH 10, and maximum uptake occurs at pH < 3. At alkaline pH, there was no uptake of gold by the pyrrhotite. The process, which was better defined for the pyrite and mackinawite surfaces also studied, involved sorption of an $AuHS^0$ complex.

Bostick and Fendorf (2003), in addition to the work on arsenite sorption on to pyrite discussed above, also studied the reaction of this species with synthetic powdered FeS. Very similar results were reported to those for pyrite, although the absorption affinity increased

with pH over the entire range studied rather than becoming constant at higher pH, as in pyrite. Again, the spectroscopic results were interpreted in terms of an FeAsS surface precipitate.

Mackinawite

Mackinawite, the tetragonal FeS (in some cases described as exhibiting a small degree of nonstoichiometry, FeS_{1-x}) is the first iron sulfide to form by precipitation from aqueous solution under a wide range of conditions. The fine-grained black sulfide occurring in the reducing environment just beneath the sediment surface in many marine environments (and resulting from reaction between detritally introduced iron minerals and sulfide generated by bacterial reduction of seawater sulfate) was formerly referred to as "amorphous FeS." However, although this material is poorly crystalline or "X-ray amorphous" due to its fine grain size, on a nanometer scale it is now known to have the mackinawite structure (Vaughan and Craig 1997). This structure, refined by Lennie et al. (1995), is characterized by layers of iron atoms tetrahedrally coordinated to sulfur and with very short Fe-Fe distances within the layers (see Makovicky, 2006 this volume). In sediments, mackinawite is always a very fine particle, transient phase that transforms to other sulfides (particularly pyrite) in the cycle of lithification. However, it is an important phase in estuarine and other near-shore marine environments, and its high level of reactivity (partly due to its small grain size and, hence, large surface area) makes it of considerable environmental interest.

Because mackinawite only occurs (and can only be synthesized) as fine particle material, many of the techniques of surface science cannot be used to study its surface chemistry. However, the EXAFS and XANES methods have been used to probe the interactions of the mackinawite surface with metal ions taken-up from solution, so as to gain understanding of the behavior of pollutants in the marine (and similar related) environments noted above. Here, by acquiring data for an appropriate absorption edge of the pollutant metal of interest, the local coordination environment of that metal (numbers and types of atoms in first, second, and sometimes further surrounding shells) can be established. Such spectroscopic studies have been combined with measurements of the uptake of the metal from an aqueous solution through contact with the mackinawite. Metal uptake has generally been determined as a function of factors such as total available dissolved metal, solution pH, or concentration of other species in solution before separation of "reacted" mackinawite for spectroscopic studies.

Interactions between the mackinawite surface and dissolved toxic heavy metals have been studied for Cu and Cd (Parkman et al. 1999), Co, Ni, Mn (Butler et al. 2006) and for Au (Widler and Seward 2002). The experiments conducted have been similar to those described above for interaction with pyrite. In terms of bulk uptake experiments, the behavior of Cu and Cd involves substantial removal of the metal up to high concentrations, without any apparent limitation, such as would be the case for saturation of surface sites (ie a linear uptake rather than the decreasing sorption associated with a Langmuir isotherm). The results of spectroscopic studies point to formation of a CdS precipitate in the case of cadmium, whereas for copper, a precipitate is again formed but of the ternary sulfide chalcopyrite ($CuFeS_2$). This unexpected result is supported by work on natural Cu-rich sulfidic sediments (Parkman et al. 1999). Preliminary results for reaction of Co, Ni and Mn with mackinawite indicate substantial removal via similar precipitation reactions for Co and Ni as described above for Cu and Cd. However, Mn behaves differently, with limited uptake at pH 7 attributed to surface complexation, and much greater uptake at pH 8 attributed to a precipitation reaction (Butler et al. 2006). In the case of gold, uptake from solutions containing up to 40 mg/kg was 100% below pH 4, whereas no uptake occurred at alkaline pH (9). XPS studies revealed that, in acid solution, a chemisorption reaction occurs at the mackinawite surface leading to reduction of the Au(I) solution complex to Au(0), and formation of surface polysulfides.

The interaction between mackinawite and dissolved arsenic is a topic of particular interest because of concerns over arsenic contamination of rivers and aquifers (see Vaughan 2006 for

a general introduction). Farquhar et al. (2002) and Wolthers et al. (2003; 2005) have studied As uptake by mackinawite. Farquhar et al. (2002) used XAS to investigate the mechanisms whereby As^{3+} and As^{5+} in aqueous solution (pH 5.5-6.5) interact with the mackinawite surface and, in line with results described above for pyrite, found evidence for the formation of outer sphere complexes for both species. Wolthers et al. (2005) conducted similar experiments using a "poorly crystalline mackinawite" regarded as more akin to the material found naturally in Recent sediments (and formerly termed "amorphous FeS"). Their results also point to outer sphere complex formation as the mechanism of interaction between arsenic solution species and the mackinawite surface.

The nuclear metals are also of obvious environmental concern, and uranium and neptunium provide contrasting examples of behavior on interaction with the mackinawite surface. Uranium, introduced as the uranyl ion, shows bulk behavior similar to that exhibited by copper, being very effectively removed from solution by mackinawite (Moyes et al. 2000). However, the environment of the metal at the FeS surface, as determined from uranium *L*-edge EXAFS data, contrasts with that of copper. As illustrated in Figure 34, the uranium is clearly bonded to oxygen with U-O distances characteristic of those expected for the uranyl ion in the first shell, and a further four bonded oxygens at 2.1-2.3 Å. Beyond these shells are further oxygens at 2.9 Å, and possibly iron at ~4 Å (Moyes et al. 2000). Because of the care taken to avoid introduction of oxygen in these experiments, it was suggested that a redox reaction takes place at the FeS surface on interaction with the uranyl ion, leading to precipitation of a U_3O_8-type phase at the surface. Support for this proposal comes from studying the spectra as a function of increasing total uranium concentrations; a systematic decrease in relative intensity of the peak at 1.79 Å which is characteristic of the uranyl species occurs and there is also a systematic decrease in the second shell U-O distance from a value of around 2.2 Å to 2.1 Å, characteristic of reduced uranium (Moyes et al. 2000).

An interesting contrast is provided by studies of the interaction of pentavalent neptunium in solution with mackinawite (Moyes et al. 2002). The uptake of neptunium from solution is relatively low (~10%) and independent of solution concentration over the range 1,000-20,000 ppm. It is also independent of

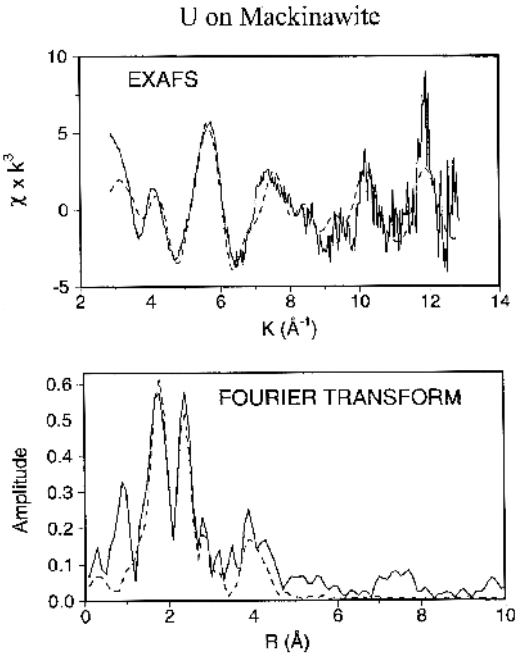

Shell	C.N.	Type	Dist. (Å)	$2\sigma^2$(Å^2)
1	2	O	1.79	0.012
2	1	O	2.12	0.002
3	3	O	2.32	0.006
4	6	O	2.90	0.040
5	4	Fe	3.96	0.022

Figure 34. EXAFS spectra, Fourier transform, and fit data results for U on mackinawite. Solid lines are the experimental data and dashed lines are best fits. The U-O bond distance of 1.79 Å is characteristic of that expected for the uranyl ion. After Moyes et al. (2000).

equilibration time. The X-ray absorption spectra for the Np *L*-edge are also essentially the same over this range of concentrations, as may be seen from their Fourier transforms in Figure 35. The best fits to these data involve an environment in which the neptunium is coordinated to four oxygen atoms at around 2.25 Å, two sulfur atoms at ~2.6 Å, and iron atoms at ~3.9 and 4.1 Å. These data suggest that, on interaction with the sulfide surface, a reduction of neptunium (V) to neptunium (IV) occurs, accompanied by a loss of axial oxygen atoms. Then, it appears that neptunium bonds directly to sulfur atoms at the FeS surface as illustrated in Figure 35. This formation of an inner sphere surface complex would explain the limited capacity of FeS to uptake neptunium, in contrast to the behavior of uranium, a result with important implications for the mobility of this element in environments where FeS occurs.

One other example of interaction of a nuclear metal with mackinawite concerns technetium, a very toxic waste product of nuclear fission with a long halflife. Under oxidizing conditions, it forms the mobile pertechnetate (TcO_4^-) anion. The reduced form of technetium, as present in technetium disulfide for example, is immobile but little is known of how technetium in solution as pertechnetate interacts with sulfidic sediments, or what might happen given subsequent re-oxidation. Exploratory work in this area at Manchester (Wharton et al. 2000; Livens et al. 2004) has employed XAS of model systems to study these problems. The technetium *K*-edge EXAFS for the pertechnetate anion show coordination to four oxygen atoms at ~1.7 Å whereas the disulfide shows coordination to six sulfur atoms at between ~2.1 and 2.5 Å. When pertechnetate is coprecipitated with FeS, the XAS data show coordination to six sulfur atoms at ~2.4 Å indicating formation of a TcS_2-like phase. However, re-oxidation of the material formed in this way does not produce a pertechnetate, but a phase with coordination to six oxygens at ~2 Å, probably a TcO_2 (and hence Tc^{4+}) phase. These observations are confirmed by the Tc *K*-edge XANES positions which are similar for TcS_2, the coprecipitate, and its re-oxidized equivalent, but clearly differ from the values for pertechnetate.

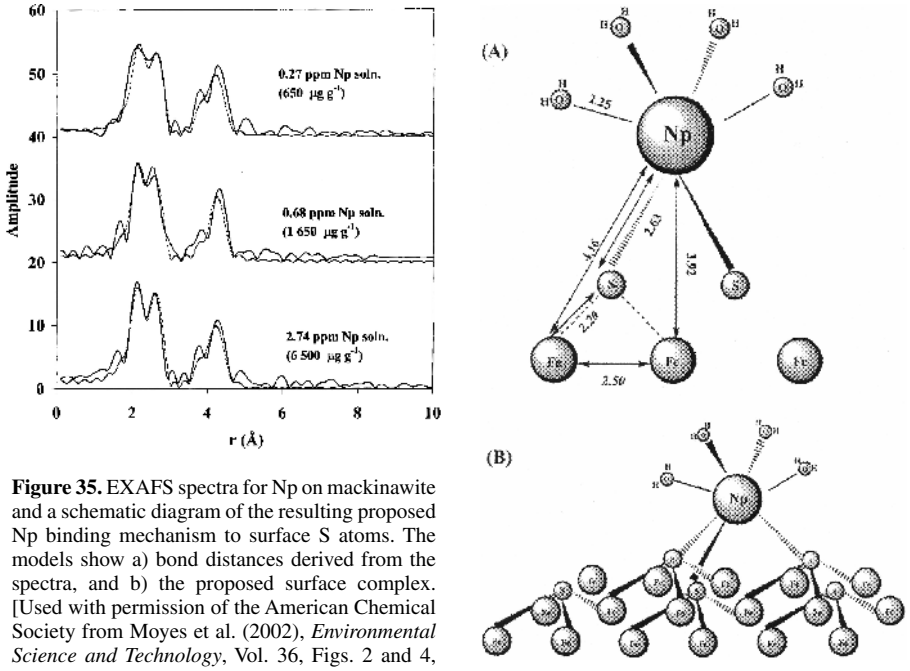

Figure 35. EXAFS spectra for Np on mackinawite and a schematic diagram of the resulting proposed Np binding mechanism to surface S atoms. The models show a) bond distances derived from the spectra, and b) the proposed surface complex. [Used with permission of the American Chemical Society from Moyes et al. (2002), *Environmental Science and Technology*, Vol. 36, Figs. 2 and 4, pp. 181 and 182.]

Sphalerite and wurtzite

Not surprisingly, ZnS has received less attention in regard to its reactions with dissolved metals than the iron sulfides. However, in a very detailed study of the interaction of the wurtzite form of ZnS with Co^{2+}, Persson et al. (1995) made wet-chemical measurements of bulk uptake and used EXAFS to probe the local environment of Co at the ZnS surface. Rather surprisingly, given the existence in nature of Co-bearing ZnS phases (see Wincott and Vaughan 2006 this volume), no evidence was found for exchange between Zn and Co. Analysis of the EXAFS results showed a first shell surrounding Co with both oxygen and sulfur atoms, and a Co-S distance of 2.36 Å which is close to the Zn-S distance in wurtzite of 2.34 Å. Surface complexation (inner sphere) of Co^{2+} to surface sulfide sites is proposed. More detailed EXAFS analysis indicated that the cobalt adsorbs to defect structural positions where Zn atoms are missing at the surface. Maximum surface complex binding capacity was estimated as 2.0 μmol m^{-2} and at increased surface coverages, a structurally disordered $Co(OH)_2$ phase is formed.

A contrasting example is provided by a quantum-mechanical study of the (110) surface of sphalerite and its interaction with Pb^{2+} solution species (Steele et al. 2003). This study was motivated by the problems caused by changes in the surface properties of sphalerite through lead "sorption" during attempts to separate it from other sulfides in mineral processing by froth flotation. These calculations show that replacement of Zn^{2+} by Pb^{2+} in the (110) surface of sphalerite is energetically unfavorable and leads to large distortions of the surface structure; also that Pb^{2+}, $PbOH^+$, $Pb(OH)_2$ and $Pb(H_2O)_2{}^{2+}$ do not bind to the surface via direct Pb-Zn or Pb-S surface bonds. The calculations do suggest that Pb^{2+} ions bind to the ZnS surface via Pb-O-Zn bonds, and that PbO, $PbOH^+$ and their inner sphere solvated complexes can bind to the surface in this way, a result in agreement with experimental evidence.

FUTURE OUTLOOK

In this chapter we have attempted to provide an overview of the main research areas and the state of understanding of the reactivity of sulfide mineral surfaces. This research area is vast and it crosscuts many scientific, engineering, and industrial domains. It also shares connections with several of the other chapters in this book. By including a wide-range of perspectives, from high vacuum surface science to the mining industry, we have tried to merge traditionally separate research fields. This merging is becoming increasingly necessary as the goal of characterizing and assessing the reactive behavior of sulfides focuses more and more on the molecular-level.

The volume of research in this area is rapidly growing, in part due to significant advances in experimental and computational tools. The availability of techniques using advanced (synchrotron) light sources has provided many new insights into the types and proportions of chemical species that evolve on sulfide surfaces during oxidation and other reactions. Scanning tunneling microscopy and spectroscopy have provided the means to dissect the surface oxidation process, or the structures of self-assembled monolayers, in terms of individual sites at the atomic level. Continual improvements in computational chemistry methods and in their efficiency provide a steady supply of increasingly accurate simulations of many kinds of reactions on sulfide surfaces. Most of these newer tools have yet to be applied across the full range of important sulfide surface chemical problems. Hence the field is currently enjoying a time when well-studied systems are being re-analyzed by application of newer tools.

Given that virtually all of the reactive behavior of sulfide minerals in the natural environment and in industrial systems is controlled by chemical reactions at their surfaces, the need to understand fundamental aspects of these reactions will be ever-present. Our dependence on mineral resources to sustain the raw material and energy needs of a growing

and developing population means that sulfide minerals, and therefore their surfaces, will continue to be exposed at the Earth's surface due to mining activities. The need to mitigate acid mine drainage and toxic metal transport, or to improve mineral extraction technologies, whether from base metal ore or coal, have been key drivers for advancing our understanding of sulfide mineral surface chemistry to its current level. While the causes of acid mine drainage are understood now better than ever, the complexity and scale of the problem will continue to provide abundant justification for improving our understanding of, for example, mechanisms and rates of sulfide oxidation reactions at molecular resolution. Similarly, improving mineral separation technologies both in terms of efficiency and affordability by investing in a molecular-level understanding of sulfide surface functionalization reactions could lead to economic and societal benefits of enormous proportions in the long term. Even though motivating factors may gradually change, given the diversity of sulfide minerals and, in some cases, the sheer volumes of the sulfides that we encounter in natural environments, we can expect that sulfide surface chemistry will persist as an important research area for many years to come.

ACKNOWLEDGMENTS

The authors gratefully acknowledge Mike Hochella for his careful review of this manuscript. KMR acknowledges the support of the U.S. Department of Energy (DOE), Office of Basic Energy Sciences, Geosciences Division, and the Stanford Environmental Molecular Sciences Institute (EMSI) jointly funded by the National Science Foundation and the DOE Office of Biological and Environmental Research (OBER). The W. R. Wiley Environmental Molecular Science Laboratory (EMSL) at Pacific Northwest National Laboratory (PNNL) is a national scientific user facility sponsored by the OBER. PNNL is operated for the DOE by Battelle Memorial Institute under contract DE-AC06-76RLO 1830. DJV acknowledges the support of the Natural Environment Research Council (NERC) in funding the Williamson Research Centre, and both the NERC and the Engineering and Physical Sciences Research Council in funding research in the mineral sciences at Manchester.

REFERENCES

Abraitis PK, Pattrick RAD, Kelsall GH, Vaughan DJ (2004) Acid leaching and dissolution of major sulphide ore minerals: processes and galvanic effects in complex systems. Mineral Mag 68:343-351

Acharya HN, Paul A (1991) Thermodynamic analysis of selective reduction of lead-oxide in galena. J Mater Sci Lett 10:257-259

Ackerman PK, Harris GH, Klimpel RR, Aplan FF (1987) Evaluation of flotation collectors for copper sulfides and pyrite .3. Effect of xanthate chain length and branching. Int J Mineral Proc 21:141-156

Allison SA, Granvill.A, Goold LA, Nicol MJ (1972) Determination of products of reaction between various sulfide minerals and aqueous xanthate solution, and a correlation of products with electrode rest potentials. Metall Trans 3:2613

Aray Y, Rodriguez J (2001) Study of hydrodesulfurization by transition metal sulfides by means of the Laplacian of the electronic charge density. Chemphyschem 2:599-604

Aray Y, Rodriguez J, Coll S, Rodriguez-Arias EN, Vega D (2005) Nature of the Lewis acid sites on molybdenum and ruthenium sulfides: An electrostatic potential study. J Phys Chem B 109:23564-23570

Aray Y, Rodriguez J, Vega D, Coll S, Rodriguez-Arias EN, Rosillo F (2002) Adsorption of thiophene on the RuS_2 (100) and (111) surfaces: A Laplacian of the electronic charge density study. J Phys Chem B 106: 13242-13249

Bancroft GM, Hyland MM (1990) Spectroscopic studies of adsorption reduction reactions of aqueous metal complexes on sulfide surfaces. Rev Mineral 23:511-558

Bang SS, Deshpande SS, Han KN (1995) The oxidation of galena using Thiobacillus Ferrooxidans. Hydromet 37:181-192

Basolo F, Pearson RG (1967) Mechanisms of Inorganic Reactions: A Study of Metal Complexes in Solution. Wiley

Becker U, Hochella MF Jr (1996) The calculation of STM images, STS spectra, and XPS peak shifts for galena: New tools for understanding mineral surface chemistry. Geochim Cosmochim Acta 60:2413-2426

Becker U, Hochella MF Jr, Vaughan DJ (1997) The adsorption of gold to galena surfaces: Calculation of adsorption/reduction energies, reaction mechanisms, XPS spectra, and STM images. Geochim Cosmochim Acta 61:3565-3585

Becker U, Rosso KM (2001) Step edges on galena (100): Probing the basis for defect driven surface reactivity at the atomic scale. Am Mineral 86:862-870

Becker U, Rosso KM, Hochella MF Jr (2001) The proximity effect on semiconducting mineral surfaces: A new aspect of mineral surface reactivity and surface complexation theory? Geochim Cosmochim Acta 65: 2641-2649

Belzile N, Chen YW, Cai MF, Li YR (2004) A review on pyrrhotite oxidation. J Geochem Explor 84:65-76

Bonnissel-Gissinger P, Alnot M, Ehrhardt JJ, Behra P (1998) Surface oxidation of pyrite as a function of pH. Environ Sci Technol 32:2839-2845

Bostick BC, Fendorf S (2003) Arsenite sorption on troilite (FeS) and pyrite (FeS_2). Geochim Cosmochim Acta 67:909-921

Bostick BC, Fendorf S, Fendorf M (2000) Disulfide disproportionation and CdS formation upon cadmium sorption on FeS_2. Geochim Cosmochim Acta 64:247-255

Bostick BC, Fendorf S, Helz GR (2003) Differential adsorption of molybdate and tetrathiomolybdate on pyrite (FeS_2). Environ Sci Technol 37:285-291

Bryce RA, Vincent MA, Hillier IH, Hall RJ (2000) Structure and stability of galena (PbS) at the interface with aqueous solution: A combined embedded cluster/reaction field study. J Molec Struct Theochem 500:169-180

Buckley AN, Walker GW (1988) The surface composition of arsenopyrite exposed to oxidizing environments. Appl Surf Sci 35:227-240

Buckley AN, Woods R (1985) X-ray photoelectron spectroscopy of oxidized pyrrhotite surfaces .1. Exposure to air. Appl Surf Sci 22-3:280-287

Buckley AN, Woods R (1987) The surface oxidation of pyrite. Appl Surf Sci 27:437-452

Buckley AN, Woods R (1991) Adsorption of ethyl xanthate on freshly exposed galena surfaces. Colloids Surf 53:33-45

Butler I, Bell R, Bell AMT, Charnock JM, Oldroyd A, Rickard DT, Vaughan DJ (2006) Co^{2+}, Ni^{2+}, Mn^{2+} uptake by mackinawite. Chem Geol (in press)

Chaturvedi S, Katz R, Guevremont J, Schoonen MAA, Strongin DR (1996) XPS and LEED study of a single-crystal surface of pyrite. Am Mineral 81:261-264

Chernyshova IV (2003) An in situ FTIR study of galena and pyrite oxidation in aqueous solution. J Electroanal Chem 558:83-98

Ciminelli VST, OsseoAsare K (1995) Kinetics of pyrite oxidation in sodium carbonate solutions. Metall Mater Trans B 26:209-218

Cincotti S, Rabe JP (1993) Self-assembled alkane monolayers on $MoSe_2$ and MoS_2. Appl Phys Lett 62:3531-3533

Costa MC, do Rego AMB, Abrantes LM (2002) Characterization of a natural and an electro-oxidized arsenopyrite: A study on electrochemical and X-ray photoelectron spectroscopy. Int J Mineral Process 65: 83-108

de Leeuw NH, Parker SC, Sithole HM, Ngoepe PE (2000) Modeling the surface structure and reactivity of pyrite: Introducing a potential model for FeS_2. J Phys Chem B 104:7969-7976

Eggleston CM (1997) Initial oxidation of sulfide sites on a galena surface: Experimental confirmation of an ab initio calculation. Geochim Cosmochim Acta 61:657-660

Eggleston CM, Ehrhardt JJ, Stumm W (1996) Surface structural controls on pyrite oxidation kinetics: An XPS-UPS, STM, and modeling study. Am Mineral 81:1036-1056

Eggleston CM, Hochella MF Jr (1990) Scanning tunneling microscopy of sulfide surfaces. Geochim Cosmochim Acta 54:1511-1517

Eggleston CM, Hochella MF Jr (1991) Scanning tunneling microscopy of galena (100) surface oxidation and sorption of aqueous gold. Science 254:983-986

Eggleston CM, Hochella MF Jr (1993) Tunneling spectroscopy applied to PbS (001) surfaces: Fresh surfaces, oxidation, and sorption of aqueous Au. Am Mineral 78:877-883

Eggleston CM, Hochella MF Jr (1994) Atomic and electronic structure of PbS (100) surfaces and chemisorption oxidation reactions. *In*: Environmental Geochemistry of Sulfide Oxidation. Alpers CN, Blowes DW (eds) American Chemical Society, p 201-222

Ehrhardt JJ, Behra P, Bonnissel-Gissinger P, Alnot M (2000) XPS study of the sorption of Hg(II) onto pyrite FeS_2. Surf Interface Anal 30:269-272

England KER, Charnock JM, Pattrick RAD, Vaughan DJ (1999) Surface oxidation studies of chalcopyrite and pyrite by glancing-angle X-ray absorption spectroscopy (REFLEXAFS). Mineral Mag 63:559-566

Evangelou VP, Seta AK, Holt A (1998) Potential role of bicarbonate during pyrite oxidation. Environ Sci Technol 32:2084-2091

Farquhar ML, Charnock JM, Livens FR, Vaughan DJ (2002) Mechanisms of arsenic uptake from aqueous solution by interaction with goethite, lepidocrocite, mackinawite, and pyrite: An X-ray absorption spectroscopy study. Environ Sci Technol 36:1757-1762

Farquhar ML, Wincott PL, Wogelius RA, Vaughan DJ (2003) Electrochemical oxidation of the chalcopyrite surface: an XPS and AFM study in solution at pH 4. Appl Surf Sci 218:34-43

Fernandez PG, Linge HG, Wadsley MW (1996a) Oxidation of arsenopyrite (FeAsS) in acid .1. Reactivity of arsenopyrite. J Appl Electrochem 26:575-583

Fernandez PG, Linge HG, Willing MJ (1996b) Oxidation of arsenopyrite (FeAsS) in acid .2. Stoichiometry and reaction scheme. J Appl Electrochem 26:585-591

Fornasiero D, Li FS, Ralston J (1994) Oxidation of galena .2. Electrokinetic study. J Colloid Interface Sci 164: 345-354

Fornasiero D, Montalti M, Ralston J (1995) Kinetics of adsorption of ethyl xanthate on pyrrhotite: In situ UV and infrared spectroscopic studies. J Colloid Interface Sci 172:467-478

Frechard F, Sautet P (1997a) Chemisorption of H_2 and H_2S on the (100) surface of RuS_2: An ab initio theoretical study. Surf Sci 389:131-146

Frechard F, Sautet P (1997b) RuS_2 (111) surfaces: Theoretical study of various terminations and their interaction with H_2. J Catal 170:402-410

Genin F, Alnot M, Ehrhardt JJ (2001) Interaction of vapours of mercury with PbS (001): A study by X-ray photoelectron spectroscopy, RHEED and X-ray absorption spectroscopy. Appl Surf Sci 173:44-53

Giancarlo LC, Fang HB, Rubin SM, Bront AA, Flynn GW (1998) Influence of the substrate on order and image contrast for physisorbed, self-assembled molecular monolayers: STM studies of functionalized hydrocarbons on graphite and MoS_2. J Phys Chem B 102:10255-10263

Grillo ME, Sautet P (2000) Density functional study of the structural and electronic properties of RuS_2 (111) II. Hydrogenated surfaces. Surf Sci 457:285-293

Grillo ME, Sautet P (2001) On the nature of RuS_2 HDS active sites: Insight from ab initio theory. J Mol Catal A 174:239-244

Guevremont JM, Strongin DR, Schoonen MAA (1997) Effects of surface imperfections on the binding of CH_3OH and H_2O on FeS_2 (100): Using adsorbed Xe as a probe of mineral surface structure. Surf Sci 391: 109-124

Guevremont JM, Bebie J, Elsetinow AR, Strongin DR, Schoonen MAA (1998a) Reactivity of the (100) plane of pyrite in oxidizing gaseous and aqueous environments: Effects of surface imperfections. Environ Sci Technol 32:3743-3748

Guevremont JM, Elsetinow AR, Strongin DR, Bebie J, Schoonen MAA (1998b) Structure sensitivity of pyrite oxidation: Comparison of the (100) and (111) planes. Am Mineral 83:1353-1356

Guevremont JM, Strongin DR, Schoonen MAA (1998c) Photoemission of adsorbed Xenon, X-ray photoemission spectroscopy, and temperature-programmed desorption studies of H_2O on FeS_2 (100). Langmuir 14:1361-1366

Guevremont JM, Strongin DR, Schoonen MAA (1998d) Thermal chemistry of H_2S and H_2O on the (100) plane of pyrite: Unique reactivity of defect sites. Am Mineral 83:1246-1255

Hacquard E, Bessiere J, Alnot M, Ehrhardt JJ (1999) Surface spectroscopic study of the adsorption of Ni(II) on pyrite and arsenopyrite at pH 10. Surf Interface Anal 27:849-860

Helveg S, Lauritsen JV, Laegsgaard E, Stensgaard I, Norskov JK, Clausen BS, Topsoe H, Besenbacher F (2000) Atomic-scale structure of single layer MoS_2 nanoclusters. Phys Rev Lett 84:951-954

Himmel HJ, Kaschke M, Harder P, Woll C (1996) Adsorption of organic monolayers on pyrite (FeS_2) (100). Thin Solid Films 285:275-280

Hochella MF Jr, Rakovan JF, Rosso KM, Bickmore BR, Rufe E (1998) New directions in mineral surface geochemical research using scanning probe microscopes. *In*: Mineral-Water Interfacial Reactions: Kinetics and Mechanisms. Sparks DL, Grundl T (eds) American Chemical Society, p 1-22

Hung A, Yarovsky I, Russo SP (2003) Density functional theory studies of xanthate adsorption on the pyrite FeS_2 (110) and (111) surfaces. J Chem Phys 118:6022-6029

Hung A, Yarovsky I, Russo SP (2004) Density functional theory of xanthate adsorption on the pyrite FeS_2 (100) surface. Phil Mag Lett 84:175-182

Janczuk B, Wojcik W, Zdziennicka A, Gonzalezcaballero F (1992a) Components of surface free energy of galena. J Mater Sci 27:6447-6451

Janczuk B, Wojcik W, Zdziennicka A, Gonzalezcaballero F (1992b) Determination of the galena surface free energy components from contact angle measurements. Mater Chem Phys 31:235-241

Jones RA, Koval SF, Nesbitt HW (2003) Surface alteration of arsenopyrite (FeAsS) by Thiobacillus ferrooxidans. Geochim Cosmochim Acta 67:955-965

Karthe S, Szargan R, Suoninen E (1993) Oxidation of pyrite surfaces: A photoelectron spectroscopic study. Appl Surf Sci 72:157-170

Kartio I, Laajalehto K, Suoninen E (1999) Characterization of the ethyl xanthate adsorption layer on galena (PbS) by synchrotron radiation excited photoelectron spectroscopy. Colloid Surf A 154:97-101

Kelsall GH, Yin Q, Vaughan DJ, England KER, Brandon NP (1999) Electrochemical oxidation of pyrite (FeS_2) in aqueous electrolytes. J Electroanal Chem 471:116-125

Kendelewicz T, Doyle CS, Bostick BC, Brown GE (2004) Initial oxidation of fractured surfaces of FeS_2 (100) by molecular oxygen, water vapor, and air. Surf Sci 558:80-88

Kendelewicz T, Liu P, Brown GE, Nelson EJ (1998) Interaction of sodium overlayers with the PbS (100) (galena) surface: Evidence for a Na <-> Pb exchange reaction. Surf Sci 411:10-22

Laajalehto K, Kartio I, Suoninen E (1997) XPS and SR-XPS techniques applied to sulphide mineral surfaces. Int J Mineral Proc 51:163-170

Lan Y, Huang X, Deng B (2002) Suppression of pyrite oxidation by iron 8-hydroxyquinoline. Arch Environ Contam Toxicol 43:168-174

Larsson ML, Holmgren A, Forsling W (2000) Xanthate adsorbed on ZnS studied by polarized FTIR-ATR spectroscopy. Langmuir 16:8129-8133

Larsson ML, Holmgren A, Forsling W (2001) Structure and orientation of collectors adsorbed at the ZnS/water interface. J Colloid Interface Sci 242:25-30

Lauritsen JV, Bollinger MV, Laegsgaard E, Jacobsen KW, Norskov JK, Clausen BS, Topsoe H, Besenbacher F (2004a) Atomic-scale insight into structure and morphology changes of MoS_2 nanoclusters in hydrotreating catalysts. J Catal 221:510-522

Lauritsen JV, Nyberg M, Norskov JK, Clausen BS, Topsoe H, Laegsgaard E, Besenbacher F (2004b) Hydrodesulfurization reaction pathways on MoS_2 nanoclusters revealed by scanning tunneling microscopy. J Catal 224:94-106

Lennie AR, Redfern SAT, Scofield PF, Vaughan DJ (1995) Synthesis and Rietveld crystal structure refinement of mackinawite, tetragonal FeS. Mineral Mag 59:677-683

Leppinen JO, Basilio CI, Yoon RH (1988) In situ FTIR spectroscopic study of ethyl xanthate electrosorption on sulfide minerals. J Electrochem Soc 135:C145-C145

Leppinen JO, Basilio CI, Yoon RH (1989) Insitu FTIR study of ethyl xanthate adsorption on sulfide minerals under conditions of controlled potential. Int J Mineral Proc 26:259-274

Leppinen JO, Rastas JK (1986) The Interaction between ethyl xanthate ion and lead sulfide surface. Colloid Surf 20:221-237

Leppinen JO, Rastas JK (1988) Thermodynamics of the system lead sulfide and thiol collector. Colloid Surf 29: 205-220

Livens FR, Jones MJ, Hynes AJ, Charnock JM, Mosselmans JFW, Hennig C, Steele H, Collison D, Vaughan DJ, Pattrick RAD, Reed WA, Moyes LN (2004) X-ray absorption spectroscopy studies of reactions of technetium, uranium and neptunium with mackinawite. J Environ Radioact 74:211-219

Lowson RT (1982) Aqueous oxidation of pyrite by molecular oxygen. Chem Rev 82:461-497

Ludwig C, Strohmaier R, Petersen J, Gompf B, Eisenmenger W (1994) Epitaxy and scanning tunneling microscopy image contrast of copper phthalocyanine on graphite and MoS_2. J Vac Sci Technol B 12: 1963-1966

Makovicky E (2006) Crystal structures of sulfides and other chalcogenides. Rev Mineral Geochem 61:7-125

Maier GS, Dobias B (1997) 2-mercaptobenzothiazole and derivatives in the flotation of galena, chalcocite and sphalerite: A study of flotation, adsorption and microcalorimetry. Mineral Eng 10:1375-1393

Mattila S, Leiro JA, Heinonen M (2004) XPS study of the oxidized pyrite surface. Surf Sci 566:1097-1101

McKibben MA, Barnes HL (1986) Oxidation of pyrite in low temperature acidic solutions: Rate laws and surface textures. Geochim Cosmochim Acta 50:1509-1520

Mielczarski JA, Mielczarski E, Zachwieja J, Cases JM (1995) In situ and ex situ infrared studies of nature and structure of thiol monolayers adsorbed on cuprous sulfide at controlled potential: Simulation and experimental results. Langmuir 11:2787-2799

Mielczarski JA, Cases JM, Alnot M, Ehrhardt JJ (1996a) XPS characterization of chalcopyrite, tetrahedrite, and tennantite surface products after different conditioning. 1. Amyl xanthate solution at pH 10. Langmuir 12: 2531-2543

Mielczarski JA, Cases JM, Alnot M, Ehrhardt JJ (1996b) XPS characterization of chalcopyrite, tetrahedrite, and tennantite surface products after different conditioning. 1. Aqueous solution at pH. Langmuir 12: 2519-2530

Mielczarski JA, Cases JM, Barres O (1996c) In situ infrared characterization of surface products of interaction of an aqueous xanthate solution with chalcopyrite, tetrahedrite, and tennantite. J Colloid Interface Sci 178: 740-748

Mielczarski JA, Mielczarski E, Cases JM (1996d) Interaction of amyl xanthate with chalcopyrite, tetrahedrite, and tennantite at controlled potentials. Simulation and spectroelectrochemical results for two-component adsorption layers. Langmuir 12:6521-6529

Mielczarski JA, Mielczarski E, Cases JM (1997) Infrared evaluation of composition and structure of ethyl xanthate monolayers produced on chalcopyrite, tetrahedrite, tennantite at controlled potentials. J Colloid Interface Sci 188:150-161

Mielczarski JA, Mielczarski E, Cases JM (1998) Influence of chain length on adsorption of xanthates on chalcopyrite. Int J Mineral Proc 52:215-231

Mikhlin Y, Tomashevich Y (2005) Pristine and reacted surfaces of pyrrhotite and arsenopyrite as studied by X-ray absorption near-edge structure spectroscopy. Phys Chem Mineral 32:19-27

Mishra KK, Osseoasare K (1992) Electroreduction Of Fe^{3+}, O_2, And $Fe(CN)_6^{3-}$ at the n-type pyrite (FeS_2) surface. J Electrochem Soc 139:3116-3120

Moses CO, Nordstrom DK, Herman JS, Mills AL (1987) Aqueous pyrite oxidation by dissolved oxygen and by ferric iron. Geochim Cosmochim Acta 51:1561-1571

Moses CO, Herman JS (1991) Pyrite oxidation at circumneutral pH. Geochim Cosmochim Acta 55:471-482

Moyes LN, Parkman RH, Charnock JM, Vaughan DJ, Livens FR, Hughes CR, Braithwaite A (2000) Uranium uptake from aqueous solution by interaction with goethite, lepidocrocite, muscovite, and mackinawite: An X-ray absorption spectroscopy study. Environ Sci Technol 34:1062-1068

Moyes LN, Jones MJ, Reed WA, Livens FR, Charnock JM, Mosselmans JFW, Hennig C, Vaughan DJ, Pattrick RAD (2002) An X-ray absorption spectroscopy study of neptunium(V) reactions with mackinawite (FeS). Environ Sci Technol 36:179-183

Mycroft JR, Bancroft GM, McIntyre NS, Lorimer JW (1995a) Spontaneous deposition of gold on pyrite from solutions containing Au(III) and Au(I) chlorides. 1. A surface study. Geochim Cosmochim Acta 59:3351-3365

Mycroft JR, Nesbitt HW, Pratt AR (1995b) X-Ray photoelectron and Auger electron spectroscopy of air oxidized pyrrhotite: Distribution of oxidized species with depth. Geochim Cosmochim Acta 59:721-733

Nesbitt HW, Bancroft GM, Pratt AR, Scaini MJ (1998) Sulfur and iron surface states on fractured pyrite surfaces. Am Mineral 83:1067-1076

Nesbitt HW, Muir IJ (1994) X-Ray photoelectron spectroscopic study of a pristine pyrite surface reacted with water vapor and air. Geochim Cosmochim Acta 58:4667-4679

Nesbitt HW, Muir IJ, Pratt AR (1995) Oxidation of arsenopyrite by air and air-saturated, distilled water, and implications for mechanism of oxidation. Geochim Cosmochim Acta 59:1773-1786

Nesbitt HW, Muir IJ (1998) Oxidation states and speciation of secondary products on pyrite and arsenopyrite reacted with mine waste waters and air. Mineral Pet 62:123-144

Nowak P (1993) Xanthate adsorption at PbS surfaces: Molecular model and thermodynamic description. Colloid Surf A 76:65-72

Parkman RH, Charnock JM, Bryan ND, Livens FR, Vaughan DJ (1999) Reactions of copper and cadmium ions in aqueous solution with goethite, lepidocrocite, mackinawite, and pyrite. Am Mineral 84:407-419

Pattrick RAD, England KER, Charnock JM, Mosselmans JFW (1999) Copper activation of sphalerite and its reaction with xanthate in relation to flotation: An X-ray absorption spectroscopy (reflection extended X-ray absorption fine structure) investigation. Int J Mineral Proc 55:247-265

Paul JF, Payen E (2003) Vacancy formation on MoS_2 hydrodesulfurization catalyst: DFT study of the mechanism. J Phys Chem B 107:4057-4064

Pearce CI, Pattrick RAD, Vaughan DJ (2006) Electrical and Magnetic properties of sulfides. Rev Mineral Geochem 61:127-180

Persson P, Parks GA, Brown GE (1995) Adsorption and structural environment of Co(II) at the zinc oxide-aqueous and zinc sulfide-aqueous solution interfaces. Langmuir 11:3782-3794

Petersen J, Strohmaier R, Gompf B, Eisenmenger W (1997) Monolayers of tetrachloro-thioindigo and thioindigo in the STM: Orientational disorder and the absence of photochromism. Surf Sci 389:329-337

Pettenkofer C, Jaegermann W, Bronold M (1991) Site specific surface interaction of electron donors and acceptors on FeS_2 (100) cleavage planes. Ber Bunsenges Phys Chem 95:560-565

Philpott MR, Goliney IY, Lin TT (2004) Molecular dynamics simulation of water in a contact with an iron pyrite FeS_2 surface. J Chem Phys 120:1943-1950

Porento M, Hirva P (2002) Theoretical studies on the interaction of anionic collectors with Cu^+, Cu^{2+}, Zn^{2+} and Pb^{2+} ions. Theor Chem Acc 107:200-205

Porento M, Hirva P (2003) The adsorption interaction of anionic sulfhydryl collectors on different PbS (100) surface sites. Surf Sci 539:137-144

Porento M, Hirva P (2004) A theoretical study on the interaction of sulfhydryl surfactants with a covellite (001) surface. Surf Sci 555:75-82

Porento M, Hirva P (2005) Effect of copper atoms on the adsorption of ethyl xanthate on a sphalerite surface. Surf Sci 576:98-106

Pratt AR, Muir IJ, Nesbitt HW (1994) X-Ray photoelectron and Auger electron spectroscopic studies of pyrrhotite and mechanism of air oxidation. Geochim Cosmochim Acta 58:827-841

Raikar GN, Thurgate SM (1991) An Auger and EELS study of oxygen adsorption on FeS_2. J Phys Cond Mater 3:1931-1939

Raybaud P, Hafner J, Kresse G, Toulhoat H (1998) Structural and electronic properties of the MoS_2 (10-10) edge surface. Surf Sci 407:237-250

Raybaud P, Hafner J, Kresse G, Kasztelan S, Toulhoat H (2000a) Ab initio study of the H_2-H_2S/MoS_2 gas-solid interface: The nature of the catalytically active sites. J Catal 189:129-146

Raybaud P, Hafner J, Kresse G, Kasztelan S, Toulhoat H (2000b) Structure, energetics, and electronic properties of the surface of a promoted MoS_2 catalyst: An ab initio local density functional study. J Catal 190:128-143

Richardson PE, Odell CS (1984) Semiconducting characteristics of galena electrodes. J Electrochem Soc 131: C99-C99

Richardson S, Vaughan DJ (1989) Arsenopyrite: A spectroscopic investigation of altered surfaces. Mineral Mag 53:223-229

Rimstidt JD, Chermak JA, Gagen PM (1994) Rates of reaction of galena, sphalerite, chalcopyrite, and arsenopyrite with Fe(III) in acidic solutions. In Environmental Geochemistry of Sulfide Oxidation. 2-13

Rimstidt JD, Vaughan DJ (2003) Pyrite oxidation: A state-of-the-art assessment of the reaction mechanism. Geochim Cosmochim Acta 67:873-880

Rosso KM, Becker U, Hochella MF Jr (1999a) Atomically resolved electronic structure of pyrite {100} surfaces: An experimental and theoretical investigation with implications for reactivity. Am Mineral 84:1535-1548

Rosso KM, Becker U, Hochella MF Jr (1999b) The interaction of pyrite {100} surfaces with O_2 and H_2O: Fundamental oxidation mechanisms. Am Mineral 84:1549-1561

Rosso KM, Becker U (2003) Proximity effects on semiconducting mineral surfaces II: Distance dependence of indirect interactions. Geochim Cosmochim Acta 67:941-953

Rosso KM, Vaughan DJ (2006) Sulfide mineral surfaces. Rev Mineral Geochem 61:505-556

Sasaki K (1994) Effect of grinding on the rate of oxidation of pyrite by oxygen in acid solutions. Geochim Cosmochim Acta 58:4649-4655

Scaini MJ, Bancroft GM, Lorimer JW, Maddox LM (1995) The interaction of aqueous silver species with sulfur-containing minerals as studied by XPS, AES, SEM, and electrochemistry. Geochim Cosmochim Acta 59: 2733-2747

Scaini MJ, Bancroft GM, Knipe SW (1997) An XPS, AES, and SEM study of the interactions of gold and silver chloride species with PbS and FeS_2: Comparison to natural samples. Geochim Cosmochim Acta 61:1223-1231

Scaini MJ, Bancroft GM, Knipe SW (1998) Reactions of aqueous Au^+ sulfide species with pyrite as a function of pH and temperature. Am Mineral 83:316-322

Schaufuss AG, Nesbitt HW, Kartio I, Laajalehto K, Bancroft GM, Szargan R (1998a) Incipient oxidation of fractured pyrite surfaces in air. J Elec Spec Rel Phen 96:69-82

Schaufuss AG, Nesbitt HW, Kartio I, Laajalehto K, Bancroft GM, Szargan R (1998b) Reactivity of surface chemical states on fractured pyrite. Surf Sci 411:321-328

Schaufuss AG, Nesbitt HW, Scaini MJ, Hoechst H, Bancroft MG, Szargan R (2000) Reactivity of surface sites on fractured arsenopyrite (FeAsS) toward oxygen. Am Mineral 85:1754-1766

Schweiger H, Raybaud P, Kresse G, Toulhoat H (2002) Shape and edge sites modifications of MoS_2 catalytic nanoparticles induced by working conditions: A theoretical study. J Catal 207:76-87

Shapter JG, Brooker MH, Skinner WM (2000) Observation of the oxidation of galena using Raman spectroscopy. Int J Mineral Proc 60:199-211

Smart RS, Jasieniak M, Prince KE, Skinner WM (2000) SIMS studies of oxidation mechanisms and polysulfide formation in reacted sulfide surfaces. Mineral Eng 13:857-870

Smelyansky V, Hafner J, Kresse G (1998) Adsorption of thiophene on RuS_2: An ab initio density functional study. Phys Rev B 58:R1782-R1785

Sowerby SJ, Heckl WM, Petersen GB (1996) Chiral symmetry breaking during the self-assembly of monolayers from achiral purine molecules. J Molec Evol 43:419-424

Sowerby SJ, Edelwirth M, Heckl WM (1998a) Self-assembly at the prebiotic solid-liquid interface: Structures of self-assembled monolayers of adenine and guanine bases formed on inorganic surfaces. J Phys Chem B 102:5914-5922

Sowerby SJ, Edelwirth M, Reiter M, Heckl WM (1998b) Scanning tunneling microscopy image contrast as a function of scan angle in hydrogen-bonded self-assembled monolayers. Langmuir 14:5195-5202

Sowerby SJ, Petersen GB (1999) Scanning tunnelling microscopy and molecular modelling of xanthine monolayers self-assembled at the solid-liquid interface: Relevance to the origin of life. Orig Life Evol Biosph 29:597-614

Steele HM, Wright K, Hillier IH (2003) A quantum-mechanical study of the (110) surface of sphalerite (ZnS) and its interaction with Pb^{2+} species. Phys Chem Mineral 30:69-75

Stirling A, Bernasconi M, Parrinello M (2003) Ab initio simulation of water interaction with the (100) surface of pyrite. J Chem Phys 118:8917-8926

Strohmaier R, Ludwig C, Petersen J, Gompf B, Eisenmenger W (1996a) Scanning tunneling microscope investigations of lead phthalocyanine on MoS_2. J Vac Sci Technol B 14:1079-1082

Strohmaier R, Ludwig C, Petersen J, Gompf B, Eisenmenger W (1996b) STM investigations of NTCDA on weakly interacting substrates. Surf Sci 351:292-302

Szargan R, Uhlig I, Wittstock G, Rossbach P (1997) New methods in flotation research: An application of synchrotron radiation to investigation of adsorbates on modified galena surfaces. Int J Mineral Proc 51: 151-161

Tan A, Harris S (1998) Electronic structure of Rh_2S_3 and RuS_2, two very active hydrodesulfurization catalysts. Inorg Chem 37:2215-2222

Tao DP, Li YQ, Richardson PE, Yoon RH (1994) The incipient oxidation of pyrite. Colloid Surf A 93:229-239

Taylor BE, Wheeler MC, Nordstrom DK (1984) Stable isotope geochemistry of acid mine drainage: Experimental oxidation of pyrite. Geochim Cosmochim Acta 48:2669-2678

Tersoff J, Hamann DR (1985) Theory of the scanning tunneling microscope. Phys Rev B 31:805-813

Todd EC, Sherman DM, Purton JA (2003) Surface oxidation of pyrite under ambient atmospheric and aqueous (pH = 2 to 10) conditions: Electronic structure and mineralogy from X-ray absorption spectroscopy. Geochim Cosmochim Acta 67:881-893

Tossell JA, Vaughan DJ (1987) Electronic structure and the chemical reactivity of the surface of galena. Can Mineral 25:381-392

Travert A, Nakamura H, van Santen RA, Cristol S, Paul JF, Payen E (2002) Hydrogen activation on Mo-based sulfide catalysts, a periodic DFT study. J Am Chem Soc 124:7084-7095

Turcotte SB, Benner RE, Riley AM, Li J, Wadsworth ME, Bodily DM (1993) Surface analysis of electrochemically oxidized metal sulfides using Raman spectroscopy. J Electroanal Chem 347:195-205

Uhlig I, Szargan R, Nesbitt HW, Laajalehto K (2001) Surface states and reactivity of pyrite and marcasite. Appl Surf Sci 179:222-229

Usher CR, Cleveland CA, Strongin DR, Schoonen MA (2004) Origin of oxygen in sulfate during pyrite oxidation with water and dissolved oxygen: An in situ horizontal attenuated total reflectance infrared spectroscopy isotope study. Environ Sci Technol 38:5604-5606

Usher CR, Paul KW, Narayansamy J, Kubicki JD, Sparks DL, Schoonen MAA, Strongin DR (2005) Mechanistic aspects of pyrite oxidation in an oxidizing gaseous environment: An in situ HATR-IR isotope study. Environ Sci Technol 39:7576-7584

Valli M, Malmensten B, Persson I (1994) Interactions between sulfide minerals and alkylxanthates .9. A vibration spectroscopic study of the interaction between arsenopyrite, millerite, molybdenite, orpiment and realgar and ethylxanthate and decylxanthate ions in aqueous solution. Colloid Surf A 83:219-225

Valli M, Persson I (1994a) Interactions between sulfide minerals and alkylxanthates. 7. A vibration and X-ray photoelectron spectroscopic study of the interaction between covellite and alkylxanthate ions and the non-sulfide mineral malachite and ethylxanthate ions in aqueous solution. Colloid Surf A 83:199-206

Valli M, Persson I (1994b) Interactions between sulfide minerals and alkylxanthates .8. A vibration and X-ray photoelectron spectroscopic study of the interaction between chalcopyrite, marcasite, pentlandite, pyrrhotite and troilite, and ethylxanthate and decylxanthate ions in aqueous solution. Colloid Surf A 83: 207-217

Vaughan DJ (ed) (2006) Arsenic. Elements 2:71-107

Vaughan DJ, England KER, Kelsall GH, Yin Q (1995) Electrochemical oxidation of chalcopyrite ($CuFeS_2$) and the related metal-enriched derivatives $Cu_4Fe_5S_8$, $Cu_9Fe_9S_{16}$, and $Cu_9Fe_8S_{16}$. Am Mineral 80:725-731

Vaughan DJ, Craig JR (1997) Sulfide ore mineral stabilities, morphologies, and intergrowth textures. *In:* Geochemistry of Hydrothermal Ore Deposits. Barnes HL (ed) Wiley, p 367-434

Velasquez P, Leinen D, Pascual J, Ramos-Barrado JR, Grez P, Gomez H, Schrebler R, Del Rio R, Cordova R (2005) A chemical, morphological, and electrochemical (XPS, SEM/EDX, CV, and EIS) analysis of electrochemically modified electrode surfaces of natural chalcopyrite ($CuFeS_2$) and pyrite (FeS_2) in alkaline solutions. J Phys Chem B 109:4977-4988

Voigt S, Szargan R, Suoninen E (1994) Interaction of copper(II) ions with pyrite and its influence on ethyl xanthate adsorption. Surf Interface Anal 21:526-536

Wharton MJ, Atkins B, Charnock JM, Livens FR, Pattrick RAD, Collison D (2000) An X-ray absorption spectroscopy study of the coprecipitation of Tc and Re with mackinawite (FeS). Appl Geochem 15:347-354

Widler AM, Seward TM (2002) The adsorption of gold(I) hydrosulphide complexes by iron sulphide surfaces. Geochim Cosmochim Acta 66:383-402

Williamson MA, Rimstidt JD (1994) The kinetics and electrochemical rate determining step of aqueous pyrite oxidation. Geochim Cosmochim Acta 58:5443-5454

Wincott PL, Vaughan DJ (2006) Spectroscopic studies of sulfides. Rev Mineral Geochem 61:181-229

Wolthers M, Charlet L, van der Weijden CH (2003) Arsenic sorption onto disordered mackinawite as a control on the mobility of arsenic in the ambient sulphidic environment. J Phys IV 107:1377-1380

Wolthers M, Charlet L, Van der Weijden CH, Van der Linde PR, Rickard D (2005) Arsenic mobility in the ambient sulfidic environment: Sorption of arsenic(V) and arsenic(III) onto disordered mackinawite. Geochim Cosmochim Acta 69:3483-3492

Wright K, Hillier IH, Vaughan DJ, Vincent MA (1999a) Cluster models of the dissociation of water on the surface of galena (PbS). Chem Phys Lett 299:527-531

Wright K, Hillier IH, Vincent MA, Kresse G (1999b) Dissociation of water on the surface of galena (PbS): A comparison of periodic and cluster models. J Chem Phys 111:6942-6946

Yin Q, Kelsall GH, Vaughan DJ, England KER (1995) Atmospheric and electrochemical oxidation of the surface of chalcopyrite ($CuFeS_2$). Geochim Cosmochim Acta 59:1091-1100

Yin Q, Vaughan DJ, England KER, Kelsall GH, Brandon NP (2000) Surface oxidation of chalcopyrite ($CuFeS_2$) in alkaline solutions. J Electrochem Soc 147:2945-2951

Zhang X, Borda MJ, Schoonen MAA, Strongin DR (2003) Adsorption of phospholipids on pyrite and their effect on surface oxidation. Langmuir 19:8787-8792

Zhang YC, Wang YX, Scanlon LG, Balbuena PB (2005) Ab initio and classical molecular dynamics studies of the dilithium phthalocyanine/pyrite interfacial structure. J Electrochem Soc 152:A1955-A1962

Zyubina TS, Neudachina VS, Yashina LV, Shtanov VI (2005) XPS and ab initio study of the interaction of PbTe with molecular oxygen. Surf Sci 574:52-64